How Far Two UAVs Should Be subject to Communication Uncertainties

Quan Quan, *Member, IEEE*, Rao Fu, and Kai-Yuan Cai

***Abstract*—Unmanned aerial vehicles are now becoming increasingly accessible to amateur and commercial users alike. A safety air traffic management system is needed to help ensure that every newest entrant into the sky does not collide with others. Much research has been done to design various methods to perform collision avoidance with obstacles. However, how to decide the safety radius subject to communication uncertainties is still suspended. Based on assumptions on communication uncertainties and supposed control performance, a separation principle of the safety radius design and controller design is proposed. With it, the safety radius in the design phase (without uncertainties) and flight phase (subject to uncertainties) are studied. Furthermore, the results are extended to multiple obstacles. Simulations and experiments are carried out to show the effectiveness of the proposed methods.**

***Index Terms*—Safety radius, swarm, collision avoidance, communication, separation principle, UAV, air traffic**

I. Introduction

A. Motivation

The number of Unmanned aerial vehicles (UAVs) continues to explode and they increasingly play an integral role in many practical applications in places where the working environment is dangerous or human capacity is limited [1]. However, in increasingly busy airspace, the conflicts among UAVs will occur frequently and become a serious problem. UAS Traffic Management (UTM) by NASA in the USA [2] and U-SPACE in the European Union [3] in progress are aiming to manage UAVs for tactical self-separation and collision avoidance [4].

Traditionally, the main role of air traffic management (ATM) is to keep a prescribed separation between all aircraft by using centralized control. However, it is infeasible for increasing UAVs because the traditional control method lacks scalability. In order to address such a problem, free flight is a developing air traffic control method that uses decentralized control [5],[6]. By Automatic Dependent Surveillance-Broadcast (ADS-B) [7], Vehicle to Vehicle (V2V) communication [8] or 5G mobile network [9], UAVs can receive the information of their neighboring obstacles to avoid collision. Especially in low-altitude airspace, utilizing the existing mobile networks will eliminate the need to deploy new infrastructure and, therefore, help to ensure connected UAVs are economically feasible [10]. Communication is often considered for UAVs, especially in the formation control, where the communication connection establishes the network topological structure [11]. However, it is not enough because communication protocols are subject to message delivery delay and packet loss. A V2V communication test on UAVs has been done by NASA for UTM showing that the probability of packet loss will be increased gradually to 1 after two UAVs keep about 1.3km away [12]. A UAV typically relies on localization sensors, monitoring systems, and/or wireless communication networks. These sensing mechanisms will provide inaccurate position information as a result of process delays, interferences, noise, and quantization, jeopardizing the safety of the vehicle and its environment [13]. If these uncertainties are not adequately taken into consideration, then UAVs may become vulnerable to collisions. This motivates us to study UAV collision avoidance problem for moving obstacles subject to sensing uncertainties, especially *communication uncertainties*.

Q. Quan, R. Fu and K-Y. Cai are with the School of Automation Science and Electrical Engineering, Beihang University, Beijing 100191, China (e-mail: qq_buaa@buaa.edu.cn; buaafurao@buaa.edu.cn; kycai@buaa.edu.cn).

B. Related Works

Much research has been done to design various methods for UAVs to perform collision avoidance with obstacles [14], including path planning [15], conflict resolution [16], model predictive control [17], motion planning of teams [18], Mixed-Integer Linear Programming (MILP) [19], potential field [20]. A simulation study of four typical collision avoidance methods can be found in [21]. Most of existing collision avoidance methods suppose that they can acquire exact sensing information. However, in recent years, more and more attention has been paid to collision avoidance subject to sensing uncertainties. Two ways are followed to extend the existing collision avoidance methods to handle sensing uncertainties for moving obstacles.

(i) The major way is to predict the future obstacles' trajectory set with uncertainty models [22],[23],[24],[25]. Then, control, decision or planning is obtained by optimization over a future time horizon to avoid obstacles' trajectory sets or reachable sets in the sense of probability. This way is often for the control methods without closed forms, like the optimization methods mentioned above. However, as pointed out in [26], under some circumstances the optimization problem may be infeasible due to the sensing uncertainties. Moreover, heavy computational burden always introduces difficulties in the design process. A discussion will be given to show this in Section IV.C. As far as we know, fewer communication uncertainties are considered in this way.

(ii) The other way is to take the sensing uncertainties into the analysis of the closed-loop of existing methods. Then, adjust controller parameters to reject uncertainties [13]. This way is often for the control methods with closed forms, like the potential field method. However, the analysis will be more difficult subject to the uncertainties like communication uncertainties. What is worse, the communication uncertainties

may make the closed-loop instability if the delay or packet loss is not compensated for elaborately [27].

C. Idea

As pointed out in [28], communication (delivery delay and packet loss) is a very significant and necessary factor that should be considered in UAV swarm. The survey paper [14] also takes communication uncertainties in collision avoidance as a challenge. To deal with sensing uncertainties including communication uncertainties, *a complementary way of collision avoidance is proposed in this paper with a principle that separates the safety radius design for uncertainties and controller design for collision avoidance*. Here, the safety radius design will take all sensing uncertainties into consideration, while the controller design does not need to take uncertainties into consideration. So, the two ways mentioned above can also benefit from the safety radius design when facing communication uncertainties. Intuitively, the safety radius will be increased as the uncertainties are increased. This is inspired by traffic rules in both the aviation area [29] and the ground transportation area [30]. For example, two airplanes should maintain standard enroute separation between aircraft (5 nautical miles (9.3 km) horizontal and 1,000 feet (300 m) vertical) [29]. Also, as shown in Figure 1, it is well known that two cars on highway should keep a certain safe distance. However, the experience to determine the safety radius for manned and airline airplanes in high-altitude airspace or safety distance for cars is difficult or not at all to apply to decentralized-control UAVs in low-altitude space because of the differences in pilot manner, communication manner, flight manner and risk requirement. On the other hand, obviously, the safety radius cannot be just the physical radius of a UAV because many uncertainties, like estimation error, communication delay and packet loss, should be considered. As pointed out in [14], the safety radius design is a challenge in the presence of sensing uncertainties, especially communication uncertainties. Moreover, the case of cooperative obstacles[1] should also be taken into consideration, which is quite different from the safety distance for cars in highway (1D space).

D. Proposed Method and Contribution

To this end, this paper focuses on studying the safety radius of decentralized-control Vertical TakeOff and Landing (VTOL) UAVs, while the deterministic collision avoidance controller could be any type as long as it satisfies certain conditions. VTOL ability, which enables easier grounding or holding by hovering, is an important ability that might be mandated by authorities in high traffic areas such as lower altitude in the urban airspace [31]. This is because VTOL drones are highly versatile and can perform tasks in an environment with very little available airspace. The study on the safety radius is divided into two phases, namely the 'offline' design phase and 'online' flight phase.

[1]The cooperative obstacles indicate that the obstacles can make collision avoidance with the UAV at the same time, such as other UAVs.

(i) In the design phase, when a UAV is on the ground, a question will arise that *how far* the UAV and an obstacle should be kept without uncertainties in order to avoid a collision in the presence of uncertainties?

(ii) On the other hand, when a UAV in the sky (in the presence of uncertainties), a question will arise that *how far* should the UAV and an obstacle be kept in the sense of estimated distance (involve uncertainties but only can be accessed) in order to avoid a collision?

To reply to these two questions, first, a VTOL UAV control model and an obstacle model are proposed. The filtered position is defined to replace position by considering velocity. Based on these models above, assumptions on practical uncertainties, like estimation error, communication delay and packet loss, are considered in the broadcast information received by the UAV. Assumptions on control performance are assumed for the design phase and the flight phase, respectively. Since only is the distance error used, the controller can be distributed. Based on these assumptions, a principle of separation of control and safety radius is proposed in the design phase (*Theorem 1*). Based on this principle, the safety radius in the design phase is derived. Then, the safety radius in the flight phase is further derived in the sense of estimated distance. These conclusions are further extended to multiple obstacles. Simulations and experiments including delay and packet loss uncertainties are carried out to show the effectiveness of the proposed method.

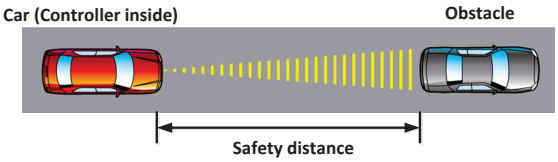

Fig. 1. Safe distance of cars in highway.

The major contribution of this paper is to separate the controller design and the safety radius so that the existing methods are available again (not need to be changed) in the presence of communication uncertainties. Concretely, the contributions of this paper are: i) a principle of separation of control and safety radius proposed so that the same controller with different safety radii can deal with different communication uncertainties; ii) safety radius derived in both the design phase and the flight phase to reduce the conservatism as much as possible; iii) filtered VTOL UAV control model in the form of a single integrator which takes the maneuverability into consideration.

The remainder of this paper is organized as follows. In Section II, the problem is formulated based on a proposed VTOL UAV control model, a proposed obstacle model, and assumptions. The solutions to the problem and their extensions are proposed in Section III. The effectiveness of the proposed safety radius design is demonstrated by simulation and flight experiments in Section IV. The conclusions are given in Section V. Some details of the mathematical proof process are given in Section VI as an appendix.

II. NOMENCLATURE

$\boldsymbol{\xi}, \mathbf{p}, \mathbf{v}, \mathbf{v}_\mathrm{c}$	Filtered position, position, velocity and velocity command of the VTOL UAV
v_m	Maximum speed of the VTOL UAV
$\hat{\boldsymbol{\xi}}, \hat{\boldsymbol{\xi}}_\mathrm{o}$	Estimated filtered position of the VTOL UAV and the obstacle
r_s,$\hat{r}_\mathrm{s}, r'_\mathrm{s}$	Safety radius, estimated safety radius and practical safety radiusof the VTOL UAV

III. PROBLEM FORMULATION

To make this paper self-contained, we introduce the modeling and some conclusions of [20]. Then, assumptions on uncertainties and control performance are proposed. Based on these models and assumptions, problems for the design and flight phase objective are formulated.

A. VTOL UAV Control Model

In a local airspace, there exists a VTOL UAV defined as

$$\mathcal{U} = \left\{ \mathbf{x} \in \mathbb{R}^3 \,|\, \|\mathbf{x} - \mathbf{p}\| < r_\mathrm{m} \right\} \tag{1}$$

where $\mathbf{p} \in \mathbb{R}^3$ is the center of mass of the UAV, $\mathcal{U}$, r_m are called the *physical area* and *physical radius* of the UAV related to its physical size, respectively. Many organizations or companies have designed some open-source semi-autonomous autopilots or offered semi-autonomous autopilots with Software Development Kits. The semi-autonomous autopilots can be used for velocity control of VTOL UAVs. With such an autopilot, the velocity of a VTOL UAV can track a given velocity command in a reasonable time. It can not only avoid the trouble of modifying the low-level source code of autopilots but also utilize commercial autopilots to complete various tasks. Based on this, the VTOL UAV satisfies the following control model

$$\begin{aligned} \dot{\mathbf{p}} &= \mathbf{v} \\ \dot{\mathbf{v}} &= -l\left(\mathbf{v} - \mathbf{v}_\mathrm{c}\right) \end{aligned} \tag{2}$$

where $l > 0$ is the velocity control gain of the VTOL UAV with the unit s^{-1}, which indicates the the VTOL UAV's maneuverability, $\mathbf{v} \in \mathbb{R}^3$ is the velocity, and $\mathbf{v}_\mathrm{c} \in \mathbb{R}^3$ is the velocity command. From the model (2), $\lim_{t\to\infty} \|\mathbf{v}(t) - \mathbf{v}_\mathrm{c}\| = 0$ if $\mathbf{v}_\mathrm{c}$ is constant. The constant l, called *maneuver constant* here, depends on the VTOL UAV and the semi-autonomous autopilot used, which can be obtained through flight experiments. It stands for the maneuverability of the VTOL UAV. If it is big, then $\mathbf{v}$ can converge to $\mathbf{v}_\mathrm{c}$ rapidly, vice versa. Here, the velocity command $\mathbf{v}_\mathrm{c}$ (required to design) for the VTOL UAV is subject to

$$\max \|\mathbf{v}_\mathrm{c}\| \le v_\mathrm{m}. \tag{3}$$

Further, the motion of each multicopter is transformed into a single integrator form to simplify the controller design and analysis. Although the distances between two UAVs in the three cases are the same, namely a marginal avoidance distance, the case in Figure 2(b) needs to carry out avoidance urgently by considering the velocity. However, the case in Figure 2(a) in fact does not need to be considered to perform collision avoidance. With such an intuition, a filtered position is defined as follows:

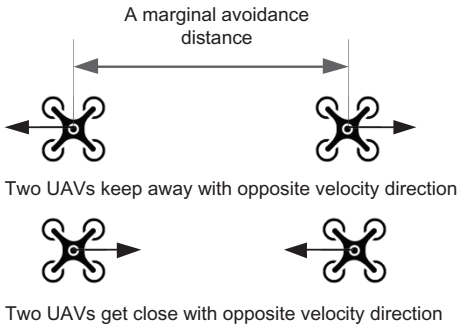

Fig. 2. Intuitive interpretation for the definition of filtered position [20].

$$\boldsymbol{\xi} \triangleq \mathbf{p} + \frac{1}{l}\mathbf{v}. \tag{4}$$

Then

$$\begin{aligned} \dot{\boldsymbol{\xi}} &= \dot{\mathbf{p}} + \frac{1}{l}\dot{\mathbf{v}} \\ &= \mathbf{v}_\mathrm{c}. \end{aligned} \tag{5}$$

Remark 1. It should be noted that the model (2) is a second-order system. By the transformation (4), the model (2) is transformed into a single integrator form to simplify the further controller design and analysis. What is more, the proposed model (2) has taken the maneuverability into consideration. Although a commonly-used model

$$\dot{\mathbf{p}} = \mathbf{v}_\mathrm{c} \tag{6}$$

is also a single integrator model, it does not take the maneuverability into consideration. As a result, the true velocity $\mathbf{v}$ will be different from $\mathbf{v}_\mathrm{c}$. The difference will be big, if the UAV's maneuverability is low. This further increases the difference between the true position and desired position especially in some situations such as making an aggressive maneuver.

Remark 2. In many pieces of literature [32],[33], the double integrator point-mass model is also employed for fixed-wing aircraft, where the desired three-dimensional velocity input $\mathbf{v}_\mathrm{c}$ subject to saturation constraints then maps to be the bank angle, thrust, and load factor for example. Therefore, the modeling of safety radius here can also be extended to fixed-wing aircraft. One significant difference is that the fixed-wing aircraft's *physical area* and *safety area* are more suitable taken as an ellipsoid. More studies are the future work.

B. Obstacle Model

In the same local airspace, there exists a moving obstacle (it may be an aircraft or a balloon) defined as

$$\mathcal{O} = \left\{ \mathbf{x} \in \mathbb{R}^3 \,|\, \|\mathbf{x} - \mathbf{p}_\mathrm{o}\| < r_\mathrm{o} \right\}$$

where $\mathbf{p}_\mathrm{o} \in \mathbb{R}^3$ is the center of mass of the obstacle, $\mathcal{O}$,r_o are called the *obstacle area* and *obstacle radius*, respectively. Define

$$\boldsymbol{\xi}_\mathrm{o} \triangleq \mathbf{p}_\mathrm{o} + \frac{1}{l}\mathbf{v}_\mathrm{o}$$

where $\mathbf{v}_{\mathrm{o}} \in \mathbb{R}^3$ is the velocity of the obstacle. The obstacle satisfies the following model

$$\max \left\| \dot{\boldsymbol{\xi}}_{\mathrm{o}} \right\| \leq v_{\mathrm{o}}$$

where $v_{\mathrm{o}} > 0$. This is a general model for any obstacle with bounded velocity and acceleration. Let

$$\dot{\boldsymbol{\xi}}_{\mathrm{o}} = \mathbf{a}_{\mathrm{o}} \tag{7}$$

with $\max \|\mathbf{a}_{\mathrm{o}}\| \leq v_{\mathrm{o}}$. Then (7) can be rewritten as

$$\begin{aligned} \dot{\mathbf{p}}_{\mathrm{o}} &= \mathbf{v}_{\mathrm{o}} \\ \dot{\mathbf{v}}_{\mathrm{o}} &= -l\left(\mathbf{v}_{\mathrm{o}} - \mathbf{a}_{\mathrm{o}}\right). \end{aligned} \tag{8}$$

In particular, if $\|\mathbf{v}_{\mathrm{o}}(0)\| \leq v_{\mathrm{o}}$ and $\mathbf{a}_{\mathrm{o}} = \mathbf{v}_{\mathrm{o}}(0)$, then the obstacle is moving with a constant velocity.

C. Assumptions on Uncertainties

Assumption 1(Estimate noise). For the UAV, the position estimate during the flight is $\boldsymbol{\xi} + \boldsymbol{\varepsilon}$, where $\|\boldsymbol{\varepsilon}\| \leq b$ and $\|\dot{\boldsymbol{\varepsilon}}\| \leq v_b$.

Assumption 2(Broadcast delay & Packet loss). The non-cooperative obstacle's information can be surveilled and then broadcasted by ground station, or be detected by airborne sensors, while the cooperative obstacle can broadcast its information to the UAV directly. The interval of receiving information for the UAV is $T_{\mathrm{s}} > 0$, while the time delay (including the broadcast period) is $0 < \tau_{\mathrm{d}} \leq \tau_{\mathrm{dm}}$. Let $\theta \in [0, 1]$ be the probability of packet loss, $\theta \leq \theta_{\mathrm{m}}$. The estimate $\hat{\boldsymbol{\xi}}_{\mathrm{o}}$ is a value that the UAV gets the estimated information from the obstacle via communication with the following model

$$\begin{aligned} \dot{\bar{\boldsymbol{\xi}}}_{\mathrm{o}}(t) &= -\frac{1-\theta}{\theta T_{\mathrm{s}}} \bar{\boldsymbol{\xi}}_{\mathrm{o}}(t) + \frac{1-\theta}{\theta T_{\mathrm{s}}} \boldsymbol{\xi}_{\mathrm{o}}(t - \tau_{\mathrm{d}}) \\ \hat{\boldsymbol{\xi}}_{\mathrm{o}}(t) &= \bar{\boldsymbol{\xi}}_{\mathrm{o}}(t) + \boldsymbol{\varepsilon}_{\mathrm{o}}, \bar{\boldsymbol{\xi}}_{\mathrm{o}}(0) = \boldsymbol{\xi}_{\mathrm{o}}(-\tau_{\mathrm{d}}) \end{aligned} \tag{9}$$

where $\|\boldsymbol{\varepsilon}_{\mathrm{o}}\| \leq b_{\mathrm{o}}$ and $\|\dot{\boldsymbol{\varepsilon}}_{\mathrm{o}}\| \leq v_{b_{\mathrm{o}}}$.

As shown in Figure 4, the value $\hat{\boldsymbol{\xi}}_{(\cdot)}$ represents the *estimated filtered position*. There exist two cases:

- Information from itself. Based on *Assumption 1*, as for the UAV itself, the filtered position estimate is

$$\hat{\boldsymbol{\xi}} = \boldsymbol{\xi} + \boldsymbol{\varepsilon} \tag{10}$$

  because no broadcast delay and packet loss need to be considered.
- Information from obstacle. The UAV has to receive information from the obstacle via communication. As shown in Figure 3, the UAV receives the information $\hat{\boldsymbol{\xi}}_{\mathrm{o}}$, which has changed by estimate noise, broadcast delay, and packet loss.

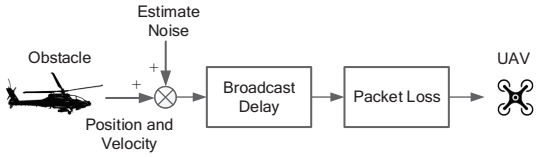

Fig. 3. Shared information broadcasting.

The relationship among the position, the filtered position and the estimated filtered position is shown in Figure 4, where the UAV cannot access the position and the filtered position (ground truth) but only the estimated filtered position including uncertainties. From the UAV's view, it senses itself and obstacle at both estimated filtered positions (dash circle) in Figure 4. If the UAV is at a high speed or the maneuver constant l is small, then true position $\mathbf{p}$ will be far from its filtered position.

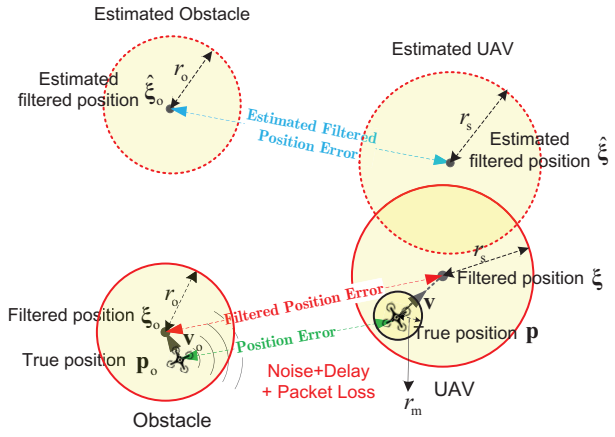

Fig. 4. Relation among position, filtered position, estimated filtered position, where the estimated filtered position will appear in (9) and (10).

Remark 2. The reasonability of the selected model (9) is explained as follows. First, a simple and reasonable estimation method is adopted

$$\hat{\boldsymbol{\xi}}_{\mathrm{o}}(t) = \begin{cases} \boldsymbol{\xi}_{\mathrm{o}}(t - \tau_{\mathrm{d}}) & \text{if data packet is received} \\ \hat{\boldsymbol{\xi}}_{\mathrm{o}}(t - T_{\mathrm{s}}) & \text{if data packet is lost} \end{cases}. \tag{11}$$

This implies that the estimate will remain the last estimated value if data packet is lost. Then, according to the probability of packet loss θ, the expected value of $\hat{\boldsymbol{\xi}}_{\mathrm{o}}$ is

$$\bar{\boldsymbol{\xi}}_{\mathrm{o}}(t) = \theta \bar{\boldsymbol{\xi}}_{\mathrm{o}}(t - T_{\mathrm{s}}) + (1-\theta)\boldsymbol{\xi}_{\mathrm{o}}(t - \tau_{\mathrm{d}}), t > 0 \tag{12}$$

where $\bar{\boldsymbol{\xi}}_{\mathrm{o}} = \mathrm{E}\left(\hat{\boldsymbol{\xi}}_{\mathrm{o}}\right)$. Roughly, the differential $\bar{\boldsymbol{\xi}}_{\mathrm{o}}$ can be written as

$$\dot{\bar{\boldsymbol{\xi}}}_{\mathrm{o}}(t) \approx \frac{\bar{\boldsymbol{\xi}}_{\mathrm{o}}(t) - \bar{\boldsymbol{\xi}}_{\mathrm{o}}(t - T_{\mathrm{s}})}{T_{\mathrm{s}}}. \tag{13}$$

Consequently, by using (13), the algebraic transformation of (12) is

$$\dot{\bar{\boldsymbol{\xi}}}_{\mathrm{o}}(t) \approx -\frac{1-\theta}{\theta T_{\mathrm{s}}} \bar{\boldsymbol{\xi}}_{\mathrm{o}}(t) + \frac{1-\theta}{\theta T_{\mathrm{s}}} \boldsymbol{\xi}_{\mathrm{o}}(t - \tau_{\mathrm{d}}).$$

Furthermore, putting uncertainties on $\boldsymbol{\varepsilon}_{\mathrm{o}}$, we have the differential equation model (9). Therefore, we can replace the model (11) with the new model (9). In the following simulation, the reasonability of the selected model (9) will be further shown.

Remark 3. The broadcast delay τ_{dm} is the maximum delay we can accept, which is the worst case. By using it, the most conservative safety radius is derived. If the delay exceeds τ_{dm}, then the packet can be considered as a loss. The time delay and the probability of packet loss are very normal parameters and can be easily measured for communication [12]. For most UAVs, filters will be used to eliminate the high-frequency

noise to preserve the low-frequency information. As a result, $b, v_b, b_{\rm o}, v_{b_{\rm o}}$ will be small.

D. Assumption on Controller

Let

$$\begin{aligned}\tilde{\mathbf{p}}_{\rm o} &\triangleq \mathbf{p}-\mathbf{p}_{\rm o}\\ \tilde{\mathbf{v}}_{\rm o} &\triangleq \mathbf{v}-\mathbf{v}_{\rm o}\\ \tilde{\boldsymbol{\xi}}_{\rm o} &\triangleq \boldsymbol{\xi}-\boldsymbol{\xi}_{\rm o}.\end{aligned} \tag{14}$$

For the UAV, no *collision* with the obstacle implies

$$\mathcal{U}\cap\mathcal{O}=\varnothing$$

namely *true position distance* $\|\tilde{\mathbf{p}}_{\rm o}\|$ satisfies

$$\|\tilde{\mathbf{p}}_{\rm o}\|\geq r_{\rm m}+r_{\rm o}. \tag{15}$$

In the following, there are two assumptions about controller design. *Assumption 3* is only for the *design phase*, during which a controller is designed for (2) without considering uncertainties to make the *filtered position distance*, namely $\left\|\tilde{\boldsymbol{\xi}}_{\rm o}\right\|$, greater than a certain distance.

Assumption 3 (Controller in Design Phase**)**. Given a *designed safety radius* $r_{\rm s}>0$, with any $\tilde{\boldsymbol{\xi}}_{\rm o}(0)$ satisfying $\left\|\tilde{\boldsymbol{\xi}}_{\rm o}(0)\right\|\geq r_{\rm s}+r_{\rm o}$, a controller

$$\mathbf{v}_{\rm c}=\mathbf{c}\left(t,\tilde{\boldsymbol{\xi}}_{\rm o}\right) \tag{16}$$

for (2) can make

$$\left\|\tilde{\boldsymbol{\xi}}_{\rm o}(t)\right\|\geq r_{\rm s}+r_{\rm o} \tag{17}$$

for any obstacle with $\left\|\dot{\boldsymbol{\xi}}_{\rm o}\right\|\leq v_{\rm m}$, where $\left\|\mathbf{c}\left(t,\tilde{\boldsymbol{\xi}}_{\rm o}\right)\right\|\leq v_{\rm m}$, for $t\geq 0$, $\forall\tilde{\boldsymbol{\xi}}_{\rm o}\in\mathbb{R}^3$.

Assumption 3 is equivalent to *Lemma 1*.

Lemma 1. If and only if

$$\min_{\mathbf{x}\in\mathcal{C}}\mathbf{x}^{\rm T}\mathbf{c}(t,\mathbf{x})\geq(r_{\rm s}+r_{\rm o})\,v_{\rm m} \tag{18}$$

then (17) holds for any obstacle $\left\|\dot{\boldsymbol{\xi}}_{\rm o}\right\|\leq v_{\rm m}$ and $\left\|\tilde{\boldsymbol{\xi}}_{\rm o}(0)\right\|\geq r_{\rm s}+r_{\rm o}$, where $\mathcal{C}=\left\{\mathbf{x}\in\mathbb{R}^3\middle|\,\|\mathbf{x}\|=r_{\rm s}+r_{\rm o}\right\}$.

Proof. The idea here relies on the following inequality

$$\min_{\mathbf{x}\in\mathcal{C}}\mathbf{x}^{\rm T}\dot{\mathbf{x}}\geq 0. \tag{19}$$

If and only if (19) holds, then $\|\mathbf{x}(t)\|\geq r_{\rm s}+r_{\rm o}$ for any $\mathbf{x}$ with $\|\mathbf{x}(0)\|\geq r_{\rm s}+r_{\rm o}$. The remaining proofs are in *Appendix*. □

In *Assumption 3*, we do not consider the uncertainties because the communication uncertainties will be left to the designed safety radius so that the same controller with different design safety radii can deal with different communication uncertainties. In the practice flight phase, $\mathbf{e}_{\rm o}$ rather than $\tilde{\boldsymbol{\xi}}_{\rm o}$ is only available. So, the same controller is used but with different feedback such as

$$\mathbf{v}_{\rm c}=\mathbf{c}(t,\mathbf{e}_{\rm o}) \tag{20}$$

for (2), where

$$\mathbf{e}_{\rm o}\triangleq\hat{\boldsymbol{\xi}}-\hat{\boldsymbol{\xi}}_{\rm o}. \tag{21}$$

Since the controller cannot get the truth, we only can make the *estimated filtered position distance*, namely $\|\mathbf{e}_{\rm o}\|$, greater than a certain distance. *Assumption 4* is only for the *flight phase* in the presence of uncertainties, describing what has happened.

Assumption 4 (Control Performance in Flight Phase**)**. There exists a *practical safety radius* $r_{\rm s}'>0$ such that, for any obstacle with $\left\|\dot{\boldsymbol{\xi}}_{\rm o}\right\|\leq v_{\rm m}$ and $\|\mathbf{e}_{\rm o}(0)\|\geq r_{\rm s}'+r_{\rm o}$, a controller for (2) can make

$$\|\mathbf{e}_{\rm o}(t)\|\geq r_{\rm s}'+r_{\rm o} \tag{22}$$

where $t\geq 0$.

E. Objective

In the 'offline' design phase (in numerical simulation), a question will arise that *how far* should the UAV and the obstacle be kept without uncertainties offline in order to avoid a collision in the presence of uncertainties?

- **Design Phase Objective (Offline)**. Under *Assumptions 1-3* and controller (16) for (2), the objective here is to determine the *estimated safety radius* $\hat{r}_{\rm s}>0$ (it is related to $r_{\rm s}$) that
$$\|\mathbf{e}_{\rm o}(t)\|\geq\hat{r}_{\rm s}+r_{\rm o} \tag{23}$$
holds, where $t\geq 0$. Furthermore, determine the designed safety radius $r_{\rm s}$ to make (15) hold in the presence of uncertainties.

On the other hand, when the UAV in practice (in the presence of uncertainties), a question will arise that *how far* should the UAV and the obstacle be kept in the sense of the estimated filtered position distance, namely $\|\mathbf{e}_{\rm o}\|$, in order to avoid a collision?

- **Flight Phase Objective (Online)**. Under *Assumptions 1-2,4*, the second objective is to determine the *practical safety radius* $r_{\rm s}'>0$ to satisfy (15).

Remark 4. The design phase objective is a type of the principle of separation of control and safety radius. It can be stated that *under some assumptions, the problem of designing a collision-avoidance controller with uncertainties can be solved by designing a safety radius covering the uncertainties, which feeds into a deterministic collision avoidance controller for the system.* Thus, the problem can be broken into two separate parts, which facilitates the design. One controller with different designed safety radii can deal with different communication uncertainties. In some cases, controllers may not satisfy *Assumption 3* but *Assumption 4* in practice. This is because the controller in *Assumption 3* considers any initial condition, or say the worst condition. But it is not necessary. For example, a UAV and an obstacle are supposed to only fly along two separate airlines without any collision avoidance control. In this case, *Assumption 3* is not satisfied, but *Assumption 4* may hold. This motivates us to consider the safety radius separately in the design phase and the flight phase.

IV. Safety Radius Design

Preliminaries are given first. By using them, the estimated safety radius and the practical safety radius are designed for the UAV and one obstacle. Furthermore, the results are extended to multiple obstacles.

A. Preliminary

First, an important lemma is proposed.

Lemma 2. Let $\mathbf{x}(t) \in \mathbb{R}^n$ and $\mathbf{y}(t) \in \mathbb{R}^n$ satisfy

$$\dot{\mathbf{x}}(t) = -k(t)\mathbf{x}(t) + k(t)\mathbf{y}(t) \tag{24}$$

where $0 < k_{\min} \leq k(t) \leq k_{\max}$. If $\|\mathbf{y}(t)\| \leq y_{\max}$, $\|\dot{\mathbf{y}}(t)\| \leq v_{y_{\max}}$, and $\|\mathbf{x}(0)\| \leq y_{\max}$, then

$$\|\mathbf{x}(t)\| \leq y_{\max}, t \geq 0. \tag{25}$$

If $\|\mathbf{x}(0) - \mathbf{y}(0)\| \leq \frac{1}{k_{\min}} v_{y_{\max}}$ holds, then

$$\|\dot{\mathbf{x}}(t)\| \leq \frac{k_{\max}}{k_{\min}} v_{y_{\max}}, t \geq 0. \tag{26}$$

Proof. See *Appendix*. □

With *Lemma 2* in hand, we have

Proposition 1. If $\|\mathbf{v}(0)\| \leq v_{\mathrm{m}}$ and the model (2) is subject to (3), then $\|\mathbf{v}(t)\| \leq v_{\mathrm{m}}$, $t \geq 0$.

Proof. It is easy from *Lemma 2*. □

According to *Proposition 1*, we have

$$\frac{1}{l}\|\tilde{\mathbf{v}}_{\mathrm{o}}\| \leq r_{\mathrm{v}} \tag{27}$$

where

$$r_{\mathrm{v}} = \frac{v_{\mathrm{m}} + v_{\mathrm{o}}}{l}. \tag{28}$$

In the following, a relationship between the true position error $\tilde{\mathbf{p}}_{\mathrm{o}}$ and the filtered position error $\tilde{\boldsymbol{\xi}}_{\mathrm{o}}$ is shown. *Proposition 2* implies that the UAV and the obstacle will be separated largely enough if their filtered position distance is separated largely enough.

Proposition 2. For the VTOL UAV and the obstacle, *if and only if* the filtered position error satisfies

$$\left\|\tilde{\boldsymbol{\xi}}_{\mathrm{o}}(t)\right\| \geq \sqrt{r^2 + r_{\mathrm{v}}^2} \tag{29}$$

and $\|\tilde{\mathbf{p}}_{\mathrm{o}}(0)\| \geq r$, then $\|\tilde{\mathbf{p}}_{\mathrm{o}}(t)\| \geq r$, where $t > 0$. The relationship "=" holds if $\frac{\mathbf{v}^{\mathrm{T}}\mathbf{v}_{\mathrm{o}}}{\|\mathbf{v}\|\|\mathbf{v}_{\mathrm{o}}\|} = -1$.

Proof. See *Appendix*. □

B. Separation Principle

For the design phase, the principle of separation of controller is stated in *Theorem 1*.

Theorem 1 (Separation Theorem). Suppose that the UAV is with model (2) under *Assumptions 1-2*. Then (i) *if and only if*

$$\left(\mathbf{e}_{\mathrm{o}}^{\mathrm{T}}\dot{\boldsymbol{\xi}} - \mathbf{e}_{\mathrm{o}}^{\mathrm{T}}\dot{\hat{\boldsymbol{\xi}}}_{\mathrm{o}}\right)\Big|_{\|\mathbf{e}_{\mathrm{o}}\| = r_{\mathrm{s}} + r_{\mathrm{o}}} \geq (r_{\mathrm{s}} + r_{\mathrm{o}}) v_b \tag{30}$$

then (23) holds with $\hat{r}_{\mathrm{s}} = r_{\mathrm{s}}$ for any $\|\mathbf{e}_{\mathrm{o}}(0)\| \geq r_{\mathrm{s}} + r_{\mathrm{o}}$; (ii) furthermore, under *Assumptions 1-3*, if

$$(r_{\mathrm{s}} + r_{\mathrm{o}})(v_{\mathrm{m}} - v_b) \geq \mathbf{e}_{\mathrm{o}}^{\mathrm{T}}\dot{\hat{\boldsymbol{\xi}}}_{\mathrm{o}}\Big|_{\|\mathbf{e}_{\mathrm{o}}\| = r_{\mathrm{s}} + r_{\mathrm{o}}} \tag{31}$$

then (23) holds with $\hat{r}_{\mathrm{s}} = r_{\mathrm{s}}$; (iii) in particular, under *Assumptions 1-3*, if

$$v_{\mathrm{m}} \geq v_{\mathrm{o}} + v_b + v_{b_{\mathrm{o}}}, \tag{32}$$

then (23) holds with $\hat{r}_{\mathrm{s}} = r_{\mathrm{s}}$.

Proof. See *Appendix*. □

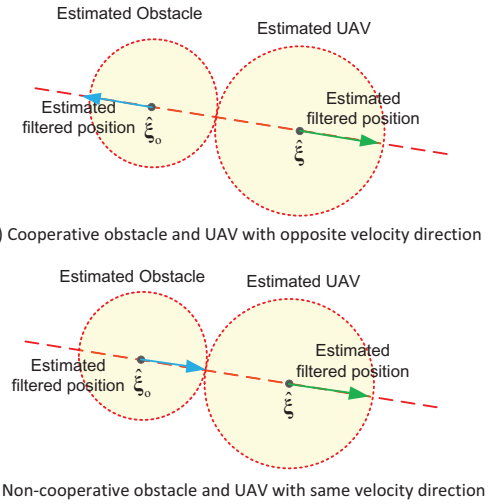

Fig. 5. A cooperative obstacle and a non-cooperative obstacle.

Remark 5. Through *Theorem 1*, we obtain $\|\mathbf{e}_{\mathrm{o}}(t)\| \geq \hat{r}_{\mathrm{s}} + r_{\mathrm{o}}$, based on which we can directly determine the lower bound of the safety radius to make UAVs safe. From now on, we do not need to consider the controller any more, because *Theorem 1* has *separated* the controller design and safety radius design. So, we call Theorem 1 as the separation theorem. It is worth pointing out that the estimated safety radius $\hat{r}_{\mathrm{s}}$ is unpredictable if Theorem 1 does not hold. In the worst case, the collision cannot be avoided. An extreme example is given in [20] that we can choose the obstacle dynamic as

$$\dot{\boldsymbol{\xi}}_{\mathrm{o}} = \dot{\boldsymbol{\xi}} - \epsilon \frac{\boldsymbol{\xi}_{\mathrm{o}} - \boldsymbol{\xi}}{\|\boldsymbol{\xi}_{\mathrm{o}} - \boldsymbol{\xi}\|} \tag{33}$$

where $\left\|\dot{\boldsymbol{\xi}}_{\mathrm{o}}\right\| \leq \left\|\dot{\boldsymbol{\xi}}\right\| + \epsilon \leq v_{\mathrm{m}} + \epsilon$ with $\epsilon > 0$. From (33), it is easy to see $\|\boldsymbol{\xi}_{\mathrm{o}}(t) - \boldsymbol{\xi}(t)\| < r_{\mathrm{s}} + r_{\mathrm{o}}$ within a finite time no matter how small ϵ is. This implies that the obstacle is chasing after the UAV and then hits it finally.

Remark 6. Let us consider a cooperative obstacle in the best case shown in Figure 5(a) and a non-cooperative obstacle in the worst case shown in Figure 5(b). The cooperative obstacle can be considered as another UAV with the same controller, namely

$$\mathbf{a}_{\mathrm{o}} = \mathbf{c}(t, -\mathbf{e}_{\mathrm{o}})$$

where, for simplicity, $-\mathbf{e}_{\mathrm{o}}$ is used for another UAV's feedback approximately. The obstacle (another UAV) will, in turn, take the UAV as its "obstacle" and will make collision avoidance simultaneously as well. According to *Lemma 1*, the following inequality

$$-\mathbf{e}_{\mathrm{o}}^{\mathrm{T}}\mathbf{c}(t, -\mathbf{e}_{\mathrm{o}})\big|_{\|\mathbf{e}_{\mathrm{o}}\| = r_{\mathrm{s}} + r_{\mathrm{o}}} \geq (r_{\mathrm{s}} + r_{\mathrm{o}}) v_{\mathrm{m}}$$

still holds. Since $\dot{\boldsymbol{\xi}}_{\mathrm{o}} = \mathbf{c}(t, -\mathbf{e}_{\mathrm{o}})$, we have

$$\mathbf{e}_{\mathrm{o}}^{\mathrm{T}}\dot{\boldsymbol{\xi}}_{\mathrm{o}}\Big|_{\|\mathbf{e}_{\mathrm{o}}\| = r_{\mathrm{s}} + r_{\mathrm{o}}} \leq -(r_{\mathrm{s}} + r_{\mathrm{o}}) v_{\mathrm{m}} < 0.$$

If $\dot{\hat{\boldsymbol{\xi}}}_{\mathrm{o}} \approx \dot{\boldsymbol{\xi}}_{\mathrm{o}}$, then $\mathbf{e}_{\mathrm{o}}^{\mathrm{T}}\dot{\hat{\boldsymbol{\xi}}}_{\mathrm{o}}\Big|_{\|\mathbf{e}_{\mathrm{o}}\| = r_{\mathrm{s}} + r_{\mathrm{o}}} < 0$. Therefore, (31) is satisfied in most cases without the requirement (32). Figure 5(a) shows the best case that the UAV and obstacle can keep

away simultaneously with the opposite direction. Intuitively, no limitation will be put on v_{o}. Figure 5(b) shows the worst case that the UAV and obstacle move simultaneously in the same direction. In this case, the requirement (32) implies that the UAV should have a faster speed than the obstacle's speed.

C. Safety Radius Design

Based on $r_{\mathrm{m}}, r_{\mathrm{o}} > 0$, we will further determine $r_{\mathrm{s}} > 0$ in order to avoid a collision in the presence of uncertainties. For this purpose, we need to analyze the relationship between the filtered position distance and the true position distance (*Proposition 2* has done), and the relationship between the filtered position distance and the estimated filtered position distance (*Proposition 3* will show), as shown in Figure 6.

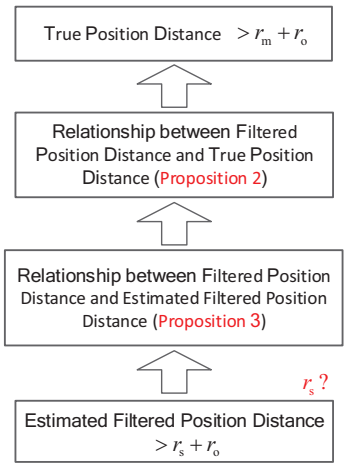

Fig. 6. Relationship from true position distance to estimated filtered position distance.

Proposition 3. Under *Assumptions 1-2*, given any $r > 0$, if

$$\|\mathbf{e}_{\mathrm{o}}(t)\| \geq r + r_e, t \geq 0 \tag{34}$$

then

$$\left\|\tilde{\boldsymbol{\xi}}_{\mathrm{o}}(t)\right\| \geq r, t \geq 0 \tag{35}$$

where

$$r_e = \frac{\theta_{\mathrm{m}} T_{\mathrm{s}}}{1-\theta_{\mathrm{m}}} v_{\mathrm{o}} + v_{\mathrm{o}} \tau_{\mathrm{dm}} + b + b_{\mathrm{o}} \tag{36}$$

Proof. See *Appendix*. □

With *Lemma 2*, we start to determine the lower bound of the safety radius r_{s} in the design phase.

Theorem 2. Under *Assumptions 1-3*, if the designed safety radius satisfies

$$r_{\mathrm{s}} \geq \sqrt{\left(r_{\mathrm{m}} + r_{\mathrm{o}}\right)^2 + r_{\mathrm{v}}^2} + r_e - r_{\mathrm{o}}, \tag{37}$$

then condition (15) holds.

Proof. According to *Proposition 3*, if

$$\|\mathbf{e}_{\mathrm{o}}(t)\| \geq r_{\mathrm{s}} + r_{\mathrm{o}}$$

then

$$\left\|\tilde{\boldsymbol{\xi}}_{\mathrm{o}}(t)\right\| \geq r_{\mathrm{s}} + r_{\mathrm{o}} - r_e.$$

If (37) holds, then

$$\left(r_{\mathrm{s}} + r_{\mathrm{o}} - r_e\right)^2 \geq \left(r_{\mathrm{m}} + r_{\mathrm{o}}\right)^2 + r_{\mathrm{v}}^2$$

namely

$$\left\|\tilde{\boldsymbol{\xi}}_{\mathrm{o}}(t)\right\| \geq \sqrt{\left(r_{\mathrm{m}} + r_{\mathrm{o}}\right)^2 + r_{\mathrm{v}}^2}.$$

According to *Proposition 2*, we have

$$\|\tilde{\mathbf{p}}_{\mathrm{o}}(t)\| \geq r_{\mathrm{m}} + r_{\mathrm{o}}.$$

□

With *Theorem 2* in hand, the solution to the flight phase objective is easy to get.

Theorem 3. Under *Assumptions 1-2,4*, if the practical safety radius satisfies

$$r_{\mathrm{s}}' \geq \sqrt{\left(r_{\mathrm{m}} + r_{\mathrm{o}}\right)^2 + r_{\mathrm{v}}^2} + r_e - r_{\mathrm{o}}$$

then (15) holds.

Proof. It is similar to the proof of *Theorem 2*. □

D. Extension to Multiple Obstacles

The results above can be extended to multiple obstacles as well. There are M obstacles

$$\mathcal{O}_{\mathrm{o},k} = \left\{\mathbf{x} \in \mathbb{R}^3 \,|\, \|\mathbf{x} - \mathbf{p}_{\mathrm{o},k}\| \leq r_{\mathrm{o}}\right\}$$

where $\mathbf{p}_{\mathrm{o},k} \in \mathbb{R}^3$ is the center position of the kth obstacle, $\mathbf{v}_{\mathrm{o},k} = \dot{\mathbf{p}}_{\mathrm{o},k} \in \mathbb{R}^3$ is the velocity of the kth obstacle, $k = 1, \cdots, M$. Define

$$\boldsymbol{\xi}_{\mathrm{o},k} \triangleq \mathbf{p}_{\mathrm{o},k} + \frac{1}{l}\mathbf{v}_{\mathrm{o},k}$$
$$\tilde{\boldsymbol{\xi}}_{\mathrm{o},k} \triangleq \boldsymbol{\xi} - \boldsymbol{\xi}_{\mathrm{o},k}.$$

These obstacles satisfy $\max \left\|\dot{\boldsymbol{\xi}}_{\mathrm{o},k}\right\| \leq v_{\mathrm{o}}$, $k = 1, \cdots, M$. For the UAV, no *collision* with the multiple obstacles implies

$$\mathcal{U} \cap \mathcal{O}_{\mathrm{o},k} = \varnothing \tag{38}$$

where $k = 1, \cdots, M$. To extend the conclusions in *Theorems 1-2* to multiple moving obstacles, we have *Assumptions 2',3'* to replace with *Assumptions 2,3* in the following.

Assumption 2' (Broadcast delay & Packet loss). The kth obstacle can be surveilled and then broadcast, or it can broadcast its information to the UAV. The interval of receiving information for the UAV is $T_{\mathrm{s}} > 0$, while the time delay (including the broadcast period) of the kth obstacle is $0 < \tau_{\mathrm{d},k} \leq \tau_{\mathrm{dm}}$. Let $\theta_k \in [0,1]$ be the probability of packet loss for the kth obstacle, $\theta_k \leq \theta_{\mathrm{m}} < 1$. The estimate $\hat{\boldsymbol{\xi}}_{\mathrm{o},k}$ is a value that the kth UAV gets the estimated information from the obstacle via communication with the following model

$$\begin{aligned}
\dot{\bar{\boldsymbol{\xi}}}_{\mathrm{o},k}(t) &= -\frac{1-\theta_k}{\theta_k T_{\mathrm{s}}}\bar{\boldsymbol{\xi}}_{\mathrm{o},k}(t) + \frac{1-\theta_k}{\theta_k T_{\mathrm{s}}}\boldsymbol{\xi}_{\mathrm{o},k}(t - \tau_{\mathrm{d},k}) \\
\hat{\boldsymbol{\xi}}_{\mathrm{o},k}(t) &= \bar{\boldsymbol{\xi}}_{\mathrm{o},k}(t) + \boldsymbol{\varepsilon}_{\mathrm{o},k}, \bar{\boldsymbol{\xi}}_{\mathrm{o},k}(0) = \boldsymbol{\xi}_{\mathrm{o},k}(-\tau_{\mathrm{d},k})
\end{aligned} \tag{39}$$

where $\|\boldsymbol{\varepsilon}_{\mathrm{o},k}\| \leq b_{\mathrm{o}}$ and $\|\dot{\boldsymbol{\varepsilon}}_{\mathrm{o},k}\| \leq v_{b_{\mathrm{o}}}$, $k = 1, \cdots, M$.

The avoidance case with multiple obstacles is complex. As stated in [20], the UAV cannot avoid collision with obstacles no matter what a controller uses under some initial conditions, such as a case shown in Figure 7. For such a purpose,

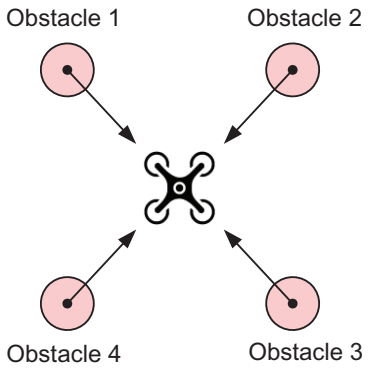

Fig. 7. A UAV surrounded by four obstacles [20].

we define a set $\mathcal{F}$ for multiple obstacles' and UAV's initial conditions in *Assumption 3'*.

Assumption 3'. Given a *designed safety radius* $r_{\rm s}>0$, with any $\left(\tilde{\boldsymbol{\xi}}_{{\rm o},1}(0),\cdots,\tilde{\boldsymbol{\xi}}_{{\rm o},M}(0)\right)\in\mathcal{F}$, a controller

$$\mathbf{v}_{\rm c}=\mathbf{c}\left(t,\tilde{\boldsymbol{\xi}}_{{\rm o},1},\cdots,\tilde{\boldsymbol{\xi}}_{{\rm o},M}\right) \tag{40}$$

for (2) can make

$$\left\|\tilde{\boldsymbol{\xi}}_{{\rm o},k}(t)\right\|\geq r_{\rm s}+r_{\rm o} \tag{41}$$

for obstacles with $\left\|\dot{\boldsymbol{\xi}}_{{\rm o},k}\right\|\leq v_{\rm o}$, where $\left\|\mathbf{c}\left(t,\tilde{\boldsymbol{\xi}}_{{\rm o},1},\cdots,\tilde{\boldsymbol{\xi}}_{{\rm o},M}\right)\right\|\leq v_{\rm m}$, for $t\geq 0$, $k=1,\cdots,M$.

Theorem 4. Suppose that the UAV is with model (2) under *Assumptions 1-2*. Then (i) if and only if

$$\left(\mathbf{e}_{{\rm o},k}^{\rm T}\dot{\boldsymbol{\xi}}-\mathbf{e}_{{\rm o},k}^{\rm T}\dot{\hat{\boldsymbol{\xi}}}_{{\rm o},k}\right)\Big|_{\|\mathbf{e}_{{\rm o},k}\|=r_{\rm s}+r_{\rm o}}\geq\left(r_{\rm s}+r_{\rm o}\right)v_b \tag{42}$$

then

$$\|\mathbf{e}_{{\rm o},k}(t)\|\geq r_{\rm s}+r_{\rm o} \tag{43}$$

for any $(\mathbf{e}_{{\rm o},1}(0),\cdots,\mathbf{e}_{{\rm o},M}(0))\in\mathcal{F}$ where $\mathbf{e}_{{\rm o},k}\triangleq\hat{\boldsymbol{\xi}}-\hat{\boldsymbol{\xi}}_{{\rm o},k}$, $k=1,\cdots,M$. (ii) In particular, under *Assumptions 1,2',3'* , if (32) holds, then (43), where $k=1,\cdots,M$. Furthermore, if $r_{\rm s}$ satisfies (37), then (38) holds for $k=1,\cdots,M$.

Proof. Proof of Conclusion (i) does not rely on *Assumption 3'*, which is similar to *Conclusion (i)* of *Theorem 1*. So, we omit it. Let us prove Conclusion (ii). The controller (40) is rewritten as

$$\begin{aligned}\mathbf{v}_{\rm c}&=\mathbf{c}\left(t,\mathbf{e}_{{\rm o},1},\cdots,\mathbf{e}_{{\rm o},M}\right)\\&=\mathbf{c}\left(t,\boldsymbol{\xi}-\boldsymbol{\xi}'_{{\rm o},1},\cdots,\boldsymbol{\xi}-\boldsymbol{\xi}'_{{\rm o},M}\right)\end{aligned}$$

where $\boldsymbol{\xi}'_{{\rm o},k}\triangleq\hat{\boldsymbol{\xi}}_{{\rm o},k}-\boldsymbol{\varepsilon}$. New obstacle $\mathcal{O}'_k$ with filtered position $\boldsymbol{\xi}'_{{\rm o},k}$ are taken into consideration, where $k=1,\cdots,M$.. If $\left(\boldsymbol{\xi}(0)-\boldsymbol{\xi}'_{{\rm o},1}(0),\cdots,\boldsymbol{\xi}(0)-\boldsymbol{\xi}'_{{\rm o},M}(0)\right)\in\mathcal{F}$ and $\left\|\dot{\boldsymbol{\xi}}'_{{\rm o},k}\right\|\leq v_{\rm o}$, then

$$\left\|\boldsymbol{\xi}-\boldsymbol{\xi}'_{{\rm o},k}\right\|\geq r_{\rm s}+r_{\rm o}$$

namely (43) holds, according to *Assumption 3'*, $k=1,\cdots,M$. The left problem is to study the condition $\left\|\dot{\boldsymbol{\xi}}'_{{\rm o},k}\right\|\leq v_{\rm m}$. The derivative $\boldsymbol{\xi}'_{{\rm o},k}$ is

$$\dot{\boldsymbol{\xi}}'_{{\rm o},k}=\dot{\tilde{\boldsymbol{\xi}}}_{{\rm o},k}+\dot{\boldsymbol{\varepsilon}}_{{\rm o},k}-\dot{\boldsymbol{\varepsilon}}. \tag{44}$$

In view of (9), according to *Lemma 1*, we have

$$\begin{aligned}\left\|\dot{\tilde{\boldsymbol{\xi}}}_{{\rm o},k}\right\|&\leq\left\|\dot{\boldsymbol{\xi}}_{{\rm o},k}\left(t-\tau_{{\rm d},k}\right)\right\|\\&\leq v_{\rm o}.\end{aligned}$$

Then, (44) is bounded as

$$\begin{aligned}\left\|\dot{\boldsymbol{\xi}}'_{{\rm o},k}\right\|&\leq\left\|\dot{\tilde{\boldsymbol{\xi}}}_{{\rm o},k}\right\|+\|\dot{\boldsymbol{\varepsilon}}_{{\rm o},k}\|+\|\dot{\boldsymbol{\varepsilon}}\|\\&\leq v_{\rm o}+v_{b_{\rm o}}+v_b\end{aligned}$$

where *Assumptions 1,2'* are utilized. Therefore, if (32) holds, then (43) holds with $\hat{r}_{\rm s}=r_{\rm s}$. □

Remark 7. The introduction to the set $\mathcal{F}$ is to make the problem completed, which is out of the scope of this paper. How to find the set $\mathcal{F}$ is an interesting problem, which can be formulated as: given a $T>0$, the initial condition set $\left(\tilde{\boldsymbol{\xi}}_{{\rm o},1}(0),\cdots,\tilde{\boldsymbol{\xi}}_{{\rm o},M}(0)\right)\in\mathcal{F}$ is a set that can make

$$\begin{aligned}&\max_{\mathbf{v}_{\rm c}}\min_{\mathbf{a}_{{\rm o},1},\cdots\mathbf{a}_{{\rm o},M}}\left(\left\|\tilde{\boldsymbol{\xi}}_{{\rm o},1}(t)\right\|,\cdots,\left\|\tilde{\boldsymbol{\xi}}_{{\rm o},M}(t)\right\|\right)\geq r_{\rm s}+r_{\rm o},0\leq t\leq T\\&\text{s.t. }\dot{\tilde{\boldsymbol{\xi}}}_{{\rm o},k}=\mathbf{v}_{\rm c}-\mathbf{a}_{{\rm o},k},\ \ \|\mathbf{v}_{\rm c}\|\leq v_{\rm m},\|\mathbf{a}_{{\rm o},k}\|\leq v_{\rm o},k=1,\cdots,M.\end{aligned}$$

Interested readers can take the problem as the feasibility of the pursuit-evasion game problem with multiple entities chasing a single target or prey [34] or group chase and escape problem [35].

To extend the conclusions in *Theorem 3* to multiple moving obstacles, we have *Assumption 4'* to replace with *Assumption 4* in the following.

Assumption 4'. There exists a practical safety radius $r'_{\rm s}>0$ such that, for obstacles with $\left\|\dot{\boldsymbol{\xi}}_{{\rm o},k}\right\|\leq v_{\rm o}$ and $\|\mathbf{e}_{{\rm o},k}(0)\|\geq r'_{\rm s}+r_{\rm o}$, a controller for (2) can make

$$\|\mathbf{e}_{{\rm o},k}(0)\|\geq r'_{\rm s}+r_{\rm o}$$

where $k=1,\cdots,M$.

In the flight phase, the results in *Theorem 3* are extended in the following *Theorem 5* for multiple obstacles.

Theorem 5. Under *Assumptions 1,2',4'*, if the practical safety radius satisfies

$$r'_{\rm s}\geq\sqrt{\left(r_{\rm m}+r_{\rm o}\right)^2+r_{\rm v}^2}+r_e-r_{\rm o}$$

then (38) holds for $k=1,\cdots,M$.

Proof. It is similar to the proof of *Theorem 3*. □

V. Simulation and Experiments

A. Simulation

The VTOL UAV's control model in the simulation scenarios are modeled as 2. In the first two simulations for avoiding non-cooperative obstacles, with the proposed separation principle (*Theorems 1,4*) and the designed safety radius (*Theorem 2*), we will show that the condition (32) is necessary in order to make avoidance subject to uncertainties. However, for cooperative obstacles which can make avoidance simultaneously, the condition (32) is not necessary, which is shown in the last simulation. The controllers [20] and [36] for UAV to avoid non-cooperative and cooperative obstacles are

Case *	b(m)	b_{o}(m)	v_b(m/s)	$v_{b_{\mathrm{o}}}$(m/s)	τ_{d}(s)	θ	r_{s}(m)
Case A	0	0	0	0	0	0	5.30
Case B	3	1	3	1	1	10%	14.30
Case C	5	2	6	5	2	20%	22.31

TABLE I
DIFFERENT COMMUNICATION PARAMETERS.

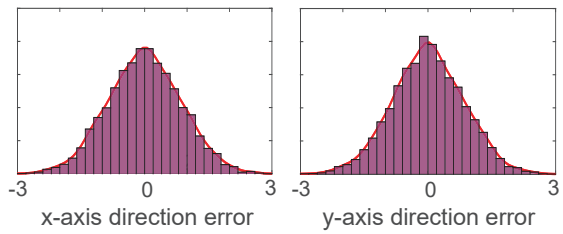

Fig. 8. Statistical property of obstacle estimate noise.

employed, respectively.[2] The results of *Theorems 3,5* can be observed directly from these results of the following simulations by choosing $\hat{r}_{\mathrm{s}} = r_{\mathrm{s}}$. A video about simulations and experiments is available on https://youtu.be/MawyB3eoZQ0 or http://t.cn/A6ZD7otD.

1) Simulation with One Non-Cooperative Obstacle:

- **Simulation Setting**. As shown in Figure 9, a scenario that one static UAV makes avoidance with one moving non-cooperative obstacle is considered. The UAV's controller to avoid non-cooperative obstacles is designed from our previous work [20], where the specific form and the proof of collision avoidance are both given. This indicates that *Assumption 3* is satisfied. Further, the simulation parameters are set as follows. The UAV with a physical radius $r_{\mathrm{m}} = 5\mathrm{m}$ is at $\mathbf{p}(0) = [0\ 0\ 100]^{\mathrm{T}}\mathrm{m}$ initially. The UAV's maneuver constant is $l = 5\mathrm{s}^{-1}$, and the maximum speed $v_{\mathrm{m}} = 10\mathrm{m/s}$. The obstacle is at $\mathbf{p}_{\mathrm{o}}(0) = [40\ 0\ 100]^{\mathrm{T}}\mathrm{m}$ initially with radius $r_{\mathrm{o}} = 10\mathrm{m}$ and a constant velocity $\mathbf{v}_{\mathrm{o}} = [-5\ 0\ 0]^{\mathrm{T}}\mathrm{m/s}$.[3] The interval of receiving information for the UAV is $T_{\mathrm{s}} = 0.01\mathrm{s}$. Communication uncertainty parameters are set as Table I, where only *Case A* has no uncertainties. We make *Case B* satisfy the condition of (32) but *Case C* not intentionally. The designed safety radii are all chosen according to (37) in *Theorem 2*.
- **Assumption Verification**. The comparison of model (9) in *Assumption 2* with the model (11) is studied by taking *Case B* as an example, where the value $\hat{\boldsymbol{\xi}}_{\mathrm{o}}$ is from (11) taking as the ground truth and $\bar{\boldsymbol{\xi}}_{\mathrm{o}}(t)$ from (9). The two models with the same communication parameters have the same input $\boldsymbol{\xi}_{\mathrm{o}}$. Let us study the noise $\boldsymbol{\varepsilon}_{\mathrm{o}} = \hat{\boldsymbol{\xi}}_{\mathrm{o}} - \bar{\boldsymbol{\xi}}_{\mathrm{o}}$. As shown in Figure 8, for the UAV, the noise $\boldsymbol{\varepsilon}_{\mathrm{o}}$ is bounded, moreover, obeying the normal distribution by Kolmogorov-Smirnov test. Therefore, *Assumption 2* is reasonable.

[2]For the convenience of reproduction, the simulation codes of this work is available at https://rfly.buaa.edu.cn/res/codes_safetyradiusdesign.rar.

[3]It should be pointing out that the change of maximum velocity of the UAV and obstacle will only affect the scale, and will not have any impact on the results in general.

- **Safety Radius Verification**. Under the initial conditions above and an obstacle avoidance controller, the *true position distance* $\|\tilde{\mathbf{p}}_{\mathrm{o}}(t)\|$ and the *estimated filtered position distance* $\|\mathbf{e}_{\mathrm{o}}(t)\|$ between the UAV and the obstacle are shown in Figure 10. Figure 10(a) corresponding to *Case A* shows that *Assumption 3* is satisfied. The results observed from Figure 9 and Figure 10(b) corresponding to *Case B*, are consistent with conclusion (iii) of *Theorem 1* and the result in *Theorem 2*. As shown in Figure 9, it should be noted that $\|\mathbf{e}_{\mathrm{o}}(t)\| \geq r_{\mathrm{s}} + r_{\mathrm{o}}$ holds consistent with conclusion (iii) in *Theorem 1* during the flight, although $\left\|\tilde{\boldsymbol{\xi}}_{\mathrm{o}}(t)\right\| < r_{\mathrm{s}} + r_{\mathrm{o}}$ after $t = 5\mathrm{s}$ because of uncertainties. Since *Case C* does not satisfy the condition of (32), as shown in Figure 10(c), $\|\mathbf{e}_{\mathrm{o}}(t)\| < r_{\mathrm{s}} + r_{\mathrm{o}}$ at time about 11.25s.

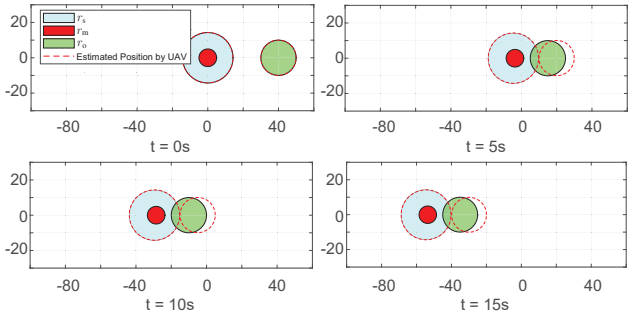

Fig. 9. Positions of UAV and obstacle at different times in Case B of numerical simulation

2) Simulation with Multiple Non-Cooperative Obstacles:

- **Simulation Setting**. As shown in Figure 11, a scenario that one UAV makes avoidance with three moving non-cooperative obstacles is considered. These obstacles can avoid each other except for the UAV. The simulation parameters are set as follows. The initial position of the UAV is set as $\mathbf{p}(0) = [0\ 40\ 100]^{\mathrm{T}}\mathrm{m}$ with radius $r_{\mathrm{m}} = 5\mathrm{m}$; the initial positions of obstacles are set as $\mathbf{p}_{\mathrm{o},1}(0) = [-40\ -40\ 100]^{\mathrm{T}}\mathrm{m}$, $\mathbf{p}_{\mathrm{o},2}(0) = [0\ -40\ 100]^{\mathrm{T}}\mathrm{m}$, $\mathbf{p}_{\mathrm{o},3}(0) = [40\ -40\ 100]^{\mathrm{T}}\mathrm{m}$ with radius $r_{\mathrm{o}} = 10\mathrm{m}$ and the velocity $v_{\mathrm{o},i} = i + 2\mathrm{m/s}$, $i = 1, 2, 3$. The others about the UAV and uncertainties are the same as those in the last simulation.
- **Safety Radius Verification**. Under the initial conditions above and an obstacle avoidance controller, the minimum *true position distance* $\min_{i\in\{1,2,3\}} \|\tilde{\mathbf{p}}_{\mathrm{o},i}(t)\|$ and the *estimated filtered position distance* $\min_{i\in\{1,2,3\}} \|\mathbf{e}_{\mathrm{o},i}(t)\|$ between the UAV and the obstacle are shown in Figure 12. Figure 12(a) corresponding to *Case A* shows that *Assumption 3'* is satisfied. The results observed from Figure 11 and Figure 12(b) corresponding to *Case B*, are consistent with conclusion (ii) of *Theorem 4*. As shown in Figure 11, it should be noted that $\min_{i\in\{1,2,3\}} \|\mathbf{e}_{\mathrm{o}}(t)\| \geq r_{\mathrm{s}} + r_{\mathrm{o}}$ holds consistent with conclusion (ii) in *Theorem 4* during the flight, although $\min_{i\in\{1,2,3\}} \left\|\tilde{\boldsymbol{\xi}}_{\mathrm{o},i}(t)\right\| < r_{\mathrm{s}} + r_{\mathrm{o}}$ about $t = 10\mathrm{s}$ because of uncertainties. Since *Case C* does not

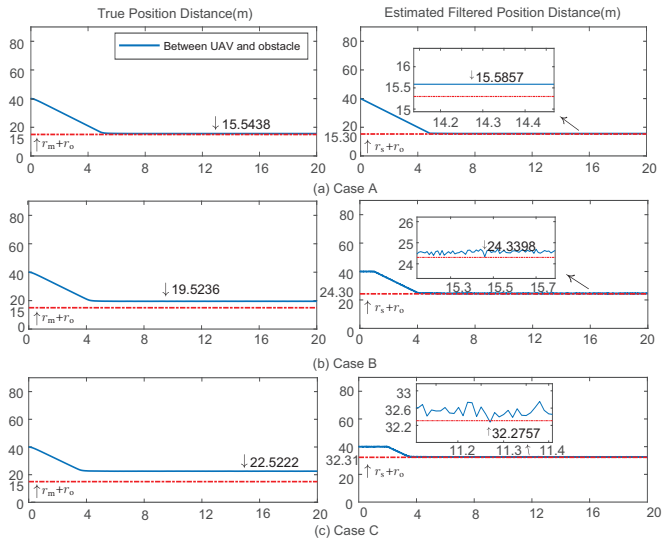

Fig. 10. The position distance and estimated filtered position distance between a UAV and one obstacle in numerical simulation.

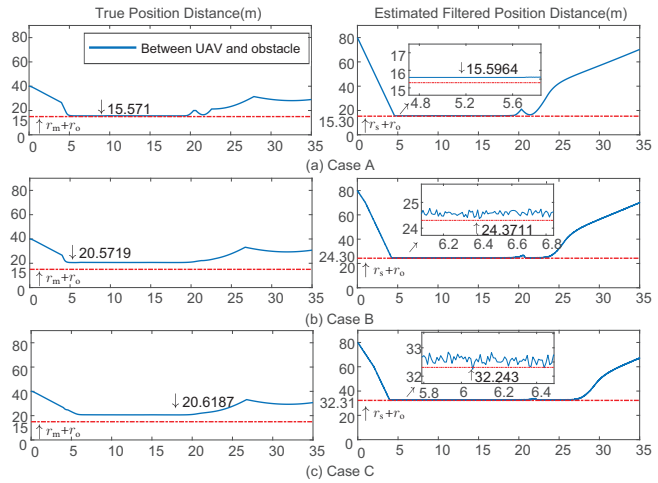

Fig. 12. Minimum position distance and estimated filtered position distance from UAV to three non-cooperative obstacles in numerical simulation.

satisfy the condition of (32), as shown in Figure 12(c), $\min_{i\in\{1,2,3\}} \|\mathbf{e}_{\mathrm{o},i}(t)\| < r_\mathrm{s} + r_\mathrm{o}$ at time about 6s.

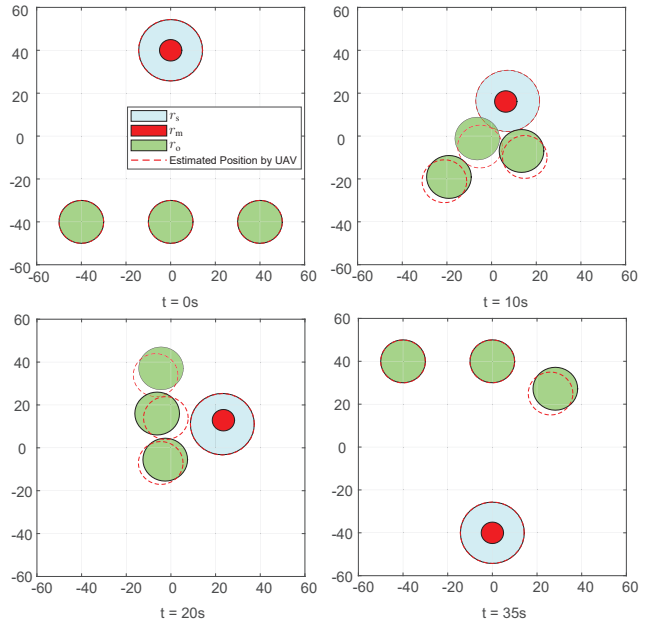

Fig. 11. Positions of UAV and three obstacles at different time in Case B of numerical simulation.

3) Simulation with Multiple Cooperative Obstacles:

- **Simulation Setting**. As shown in Figure 13, a scenario that one UAV makes avoidance with three moving cooperative obstacles is considered. The UAV and these obstacles can avoid each other. The UAV and cooperative obstacles adpot the same distributed control protocol designed from our previous work [36], where the specific form and the proof of inter-agent collision avoidance are both given. This indicates that *Assumption 3* is satisfied. The simulation parameters are set as follows. The initial position of the UAV is set as $\mathbf{p}(0) = [-40\ 40\ 100]^\mathrm{T}\mathrm{m}$ with radius $r_\mathrm{m} = 5\mathrm{m}$. The UAV's maneuver constant is $l = 5\mathrm{s}^{-1}$, and the maximum speed $v_\mathrm{m} = 5\mathrm{m/s}$. The interval of receiving information for the UAV is $T_\mathrm{s} = 0.01\mathrm{s}$. The initial positions of obstacles are set as $\mathbf{p}_{\mathrm{o},1}(0) = [40\ 40\ 100]^\mathrm{T}\mathrm{m}$, $\mathbf{p}_{\mathrm{o},2}(0) = [40\ -40\ 100]^\mathrm{T}\mathrm{m}$, $\mathbf{p}_{\mathrm{o},3}(0) = [-40\ -40\ 100]^\mathrm{T}\mathrm{m}$ with radius $r_\mathrm{o} = 10\mathrm{m}$ and their velocities $v_{\mathrm{o},i} = i + 2\mathrm{m/s}$, $i = 1, 2, 3$. Communication uncertainty parameters are set as *Case B* in Table I. The designed safety radius is chosen as $r_\mathrm{s} = 14.14\mathrm{m}$ according to (37) in *Theorem 2*. It is worth noting that the condition of (32) does not satisfy because of $v_\mathrm{m} = v_{\mathrm{o},3}$.
- **Safety Radius Verification**. Under the initial conditions above and an obstacle avoidance controller, the minimum *true position distance* $\min_{i\in\{1,2,3\}} \|\tilde{\mathbf{p}}_{\mathrm{o},i}(t)\|$ and the *estimated filtered position distance* $\min_{i\in\{1,2,3\}} \|\mathbf{e}_{\mathrm{o},i}(t)\|$ from the UAV to these obstacles are shown in Figure 14. Since the obstacles and the UAV can make collision avoidance with each other, the separation principle still holds even if $v_\mathrm{m} = v_{\mathrm{o},3}$. For a simple case, *Remark 5* has explained the reason. Consequently, $\min_{i\in\{1,2,3\}} \|\mathbf{e}_\mathrm{o}(t)\| \geq r_\mathrm{s} + r_\mathrm{o}$ holds during the flight observed from Figure 13.

B. Experiments

A motion capture system called OptiTrack is installed, from which we can get the ground truth of the position, velocity and, orientation of each multicopter. The laptop is connected to these multicopters and OptiTrack by a local network, providing the proposed controller and a real-time position plotting module. In the first experiment for a non-cooperative obstacle, with the proposed separation principle (*Theorem 1*) and designed safety radius (*Theorem 2*), we will show that the condition (32) can make avoidance subject to uncertainties. However, for cooperative obstacles which can make avoidance simultaneously, the condition (32) is not necessary, which is shown in the last two experiments. The results of *Theorems 3,5*

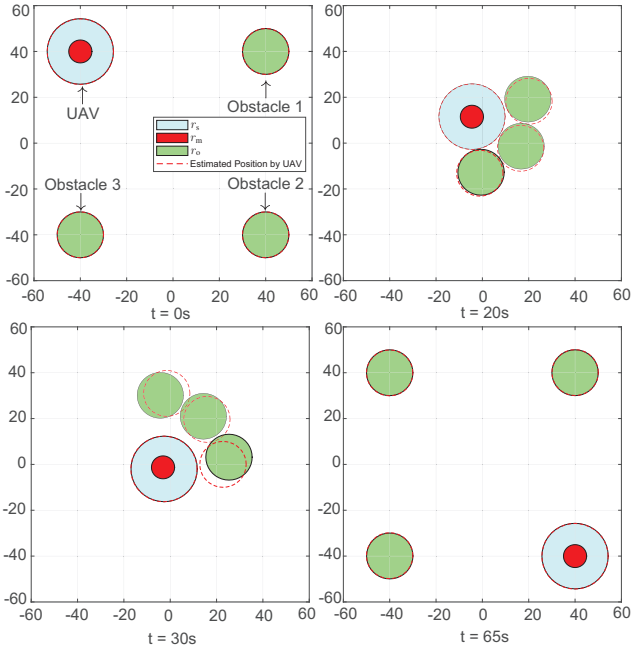

Fig. 13. Positions of UAV and three obstacles at different times in Case B of numerical simulation.

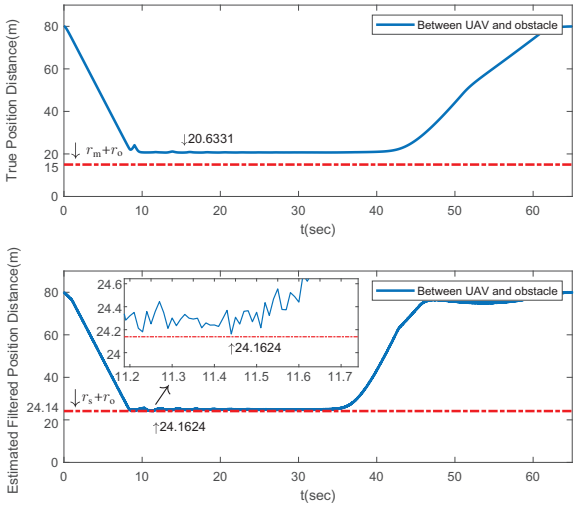

Fig. 14. Minimum position distance and filtered position distance from UAV to three cooperative obstacles in numerical simulation.

can be observed directly from these results of the following experiments by choosing $\hat{r}_{\mathrm{s}} = r_{\mathrm{s}}$.

1) Experiment with One Non-Cooperative Hovering Obstacle:

- **Experiment Setting**. An experiment scenario that one UAV makes avoidance with one non-cooperative hovering obstacle is considered. The experiment parameters are set as follows. The UAV with physical radius $r_{\mathrm{m}} = 0.2\mathrm{m}$ is at $\mathbf{p}(0) = [1.5\ 0\ 1]^{\mathrm{T}}\mathrm{m}$ initially. The UAV's maneuver constant is $l = 2\mathrm{s}^{-1}$, and the maximum speed $v_{\mathrm{m}} = 0.1\mathrm{m/s}$. The obstacle is at $\mathbf{p}_{\mathrm{o}}(0) = [-0.2\ 0\ 1]^{\mathrm{T}}\mathrm{m}$ initially with radius $r_{\mathrm{o}} = 0.2\mathrm{m}$. The interval of receiving information for the UAV is $T_{\mathrm{s}} = 0.01\mathrm{s}$. Communication uncertainty parameters are set as $b = 0.10\mathrm{m}$, $b_{\mathrm{o}} = 0.03\mathrm{m}$, $v_b = 0.08\mathrm{m/s}$, $v_{b_{\mathrm{o}}} = 0.01\mathrm{m/s}$, $\tau_{\mathrm{d}} = 1\mathrm{s}$, $\theta = 10\%$. The condition of (32) in *Theorem 2* is satisfied in this scenario. The safety radius $r_{\mathrm{s}} = 0.47\mathrm{m}$ is designed with such defined parameters according to *Theorem 2*.
- **Safety Radius Verification**. Under the initial conditions above and an obstacle avoidance controller, the true position distance and the estimated filtered position distance from the UAV to the obstacle are shown in Figure 15. The positions of multicopters during the whole flight experiment are shown in Figure 16. The UAV can complete its route at about 77s, keeping a safe distance from the obstacle without conflict. This is consistent with the separation principle (*Theorem 1*) with the designed safety radius (*Theorem 2*).

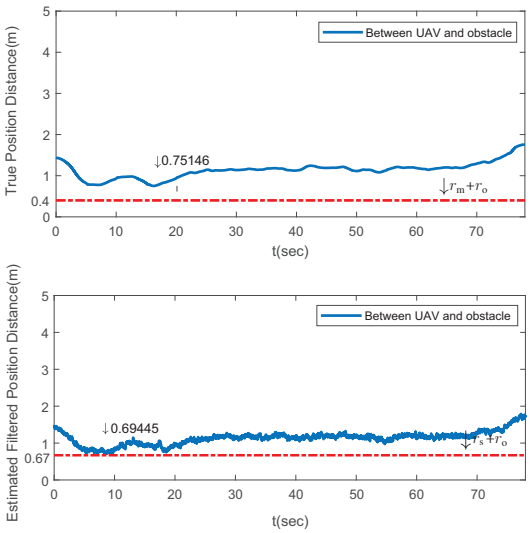

Fig. 15. The position distance and estimated filtered position distance between a UAV and one hovering obstacle in the flight experiment

2) Experiment with One Cooperative Moving Obstacle:

- **Experiment Setting**. An experiment scenario that one static UAV makes avoidance with one moving cooperative obstacle is considered. The experiment parameters are set as follows. The UAV with physical radius $r_{\mathrm{m}} = 0.2\mathrm{m}$ is at $\mathbf{p}(0) = [1.5\ 0\ 1]^{\mathrm{T}}\mathrm{m}$ initially. The UAV's maneuver constant is $l = 2\mathrm{s}^{-1}$, and the maximum speed $v_{\mathrm{m}} = 0.1\mathrm{m/s}$. The obstacle is at $\mathbf{p}_{\mathrm{o}}(0) = [-1.5\ 0\ 1]^{\mathrm{T}}\mathrm{m}$ initially with radius $r_{\mathrm{o}} = 0.2\mathrm{m}$ and $v_{\mathrm{o}} = 0.1\mathrm{m/s}$. The interval of receiving information for the UAV is $T_{\mathrm{s}} = 0.01\mathrm{s}$. Communication uncertainty parameters are set as $b = 0.2\mathrm{m}$, $b_{\mathrm{o}} = 0.1\mathrm{m}$, $v_b = 0.08\mathrm{m/s}$, $v_{b_{\mathrm{o}}} = 0.01\mathrm{m/s}$, $\tau_{\mathrm{d}} = 2\mathrm{s}$, $\theta = 30\%$. The safety radius $r_{\mathrm{s}} = 0.71\mathrm{m}$ is designed with such defined parameters by *Theorem 4*.
- **Safety Radius Verification**. Under the initial conditions above and an obstacle avoidance controller, the true position distance and the estimated filtered position distance from the UAV to the obstacle are shown in Figure 17. The positions of multicopters during the whole flight experiment are shown in Figure 18. Since the obstacle and the UAV can make collision avoidance with each other, the separation principle still holds even if

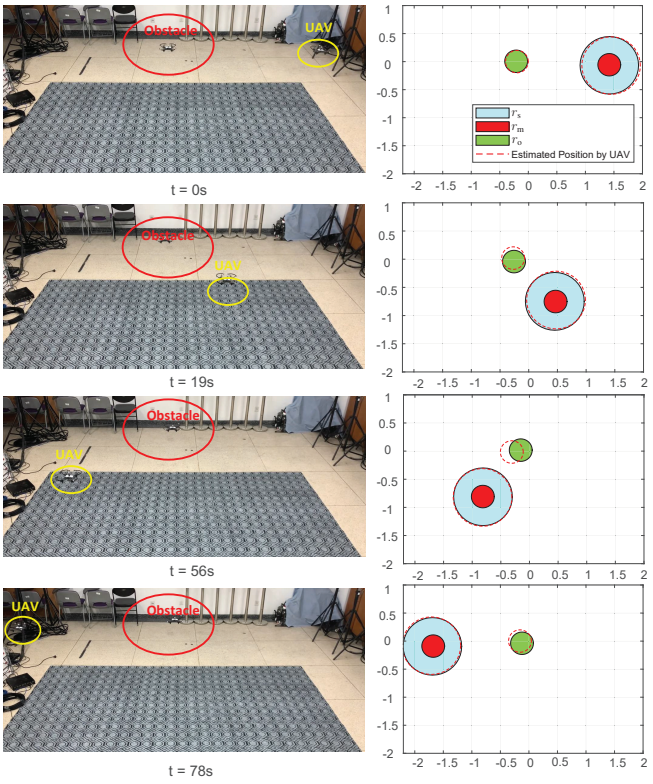

Fig. 16. Positions of a UAV and a non-cooperative hovering obstacle at different times in the flight experiment.

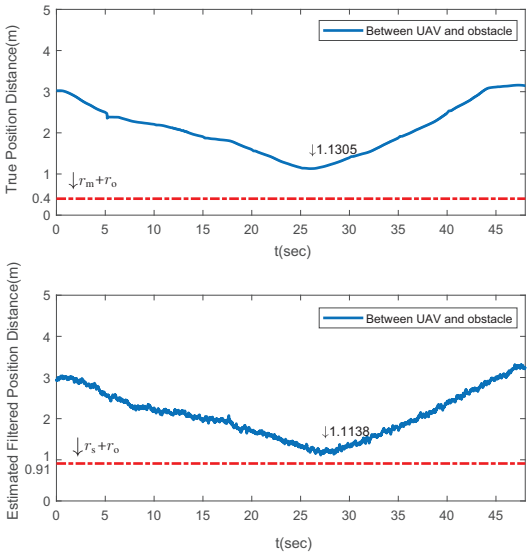

Fig. 17. The position distance and estimated filtered position distance between a UAV and one moving obstacle in the flight experiment

$v_{\rm m} = v_{\rm o}$. *Remark 5* has explained the reason. This is consistent with the separation principle (*Theorem 1*) with the designed safety radius (*Theorem 2*).

3) Experiment with Multiple Cooperative Obstacles:

- **Experiment Setting**. An experiment scenario that one UAV makes avoidance with three moving cooperative obstacles is considered. The experiment parameters are set as follows. The UAV with a physical radius $r_{\rm m} = 0.2$m is at $\mathbf{p}(0) = [-1\ 1\ 1]^{\rm T}$m initially. The UAV's maneuver constant is $l = 2$, and the maximum speed $v_{\rm m} = 0.1$m/s. The obstacles are at $\mathbf{p}_{{\rm o},1}(0) = [1\ 1\ 1]^{\rm T}$m, $\mathbf{p}_{{\rm o},2}(0) = [1\ -1\ 1]^{\rm T}$m, $\mathbf{p}_{{\rm o},3}(0) = [-1\ -1\ 1]^{\rm T}$m initially with radius $r_{\rm o} = 0.23$m and $v_{\rm o} = 0.1$m/s. The interval of receiving information for the UAV is $T_{\rm s} = 0.01$s. Communication uncertainty parameters are set as $b = 0.012$m, $b_{\rm o} = 0.01$m, $v_b = 0.012$m/s, $v_{b_{\rm o}} = 0.01$m/s, $\tau_{\rm d} = 0.1$s, $\theta = 1\%$. The safety radius $r_{\rm s} = 0.23$m is designed according to *Theorem 2*.
- **Safety Radius Verification**. Under the initial conditions above and an obstacle-avoidance controller, the minimum *true position distance* $\min\limits_{i\in\{1,2,3\}} \|\tilde{\mathbf{p}}_{{\rm o},i}(t)\|$ and the *estimated filtered position distance* $\min\limits_{i\in\{1,2,3\}} \|\mathbf{e}_{{\rm o},i}(t)\|$ from the UAV to these obstacles are shown in Figure 19. Since these obstacles and the UAV can make collision avoidance with each other, the separation principle still holds even if $v_{\rm m} = v_{\rm o}$. Consequently, $\min\limits_{i\in\{1,2,3\}} \|\mathbf{e}_{\rm o}(t)\| \geq r_{\rm s}+r_{\rm o}$ holds during the flight observed from Figure 19.

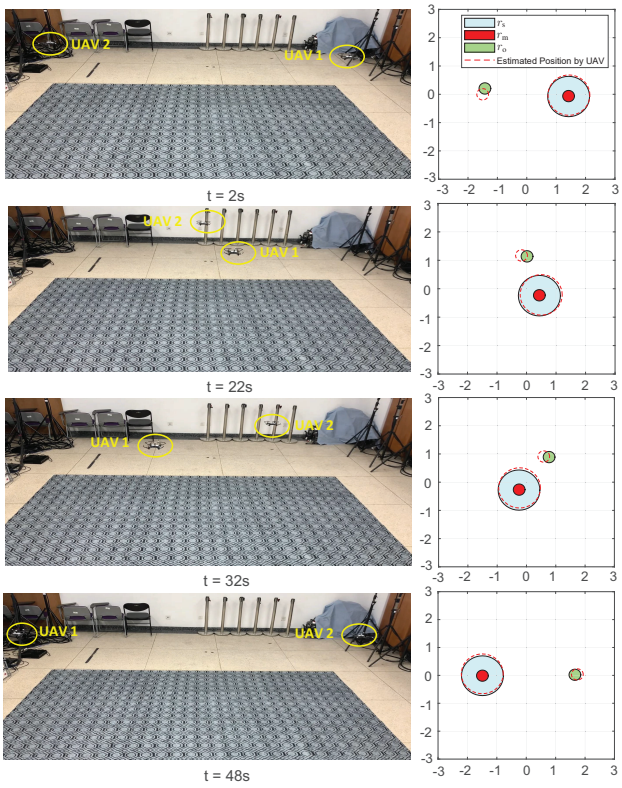

Fig. 18. Positions of UAV and a moving cooperative obstacle at different times in the flight experiment

C. Discussion

In *Assumption 3*, we proposed some requirements on the controller performance without considering the communication uncertainties. For multi-agent systems, the current control methods mainly include the *optimal trajectory method* and *forcefield-based method*. By simulation and analysis, the

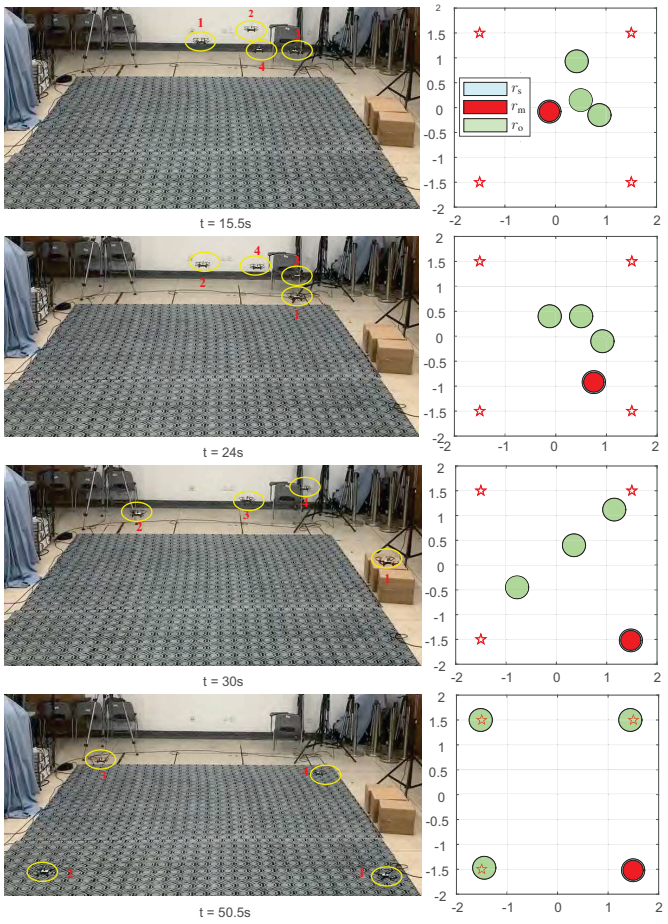

Fig. 19. Positions of four UAVs at different time in flight experiment.

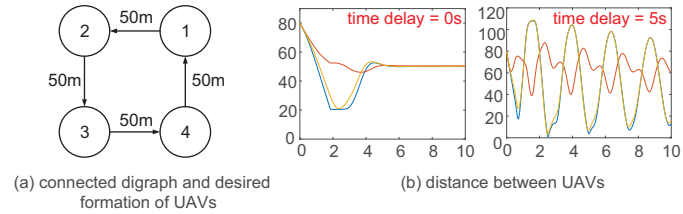

Fig. 20. Performance of formation control method subject to communication uncertainties.

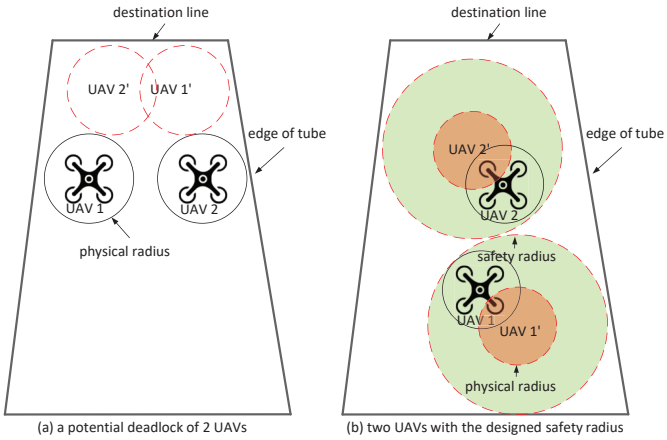

Fig. 21. Positions of two UAVs without and with the designed safety radius.

performance of different control methods subject to communication uncertainties is shown.

1) Forcefield-Based Control without Safety Radius Design: The impact of communication uncertainties on forcefield-based control is first shown by an example of formation control. The objective of the formation control method requires agents maintaining a certain formation. In [37], existing results of the formation control were introduced and categorized. We choose a simple and classical displacement-based control method to show the ability of the formation control method subject to communication uncertainties. The UAV's maneuver constant is $l = 5$, and the maximum speed $v_{\mathrm{m}} = 10$m/s. The initial positions of UAVs are set as $\mathbf{p}_1(0) = [-40\ 40\ 100]^{\mathrm{T}}$m, $\mathbf{p}_2(0) = [40\ 40\ 100]^{\mathrm{T}}$m, $\mathbf{p}_3(0) = [40\ -40\ 100]^{\mathrm{T}}$m, $\mathbf{p}_4(0) = [-40\ -40\ 100]^{\mathrm{T}}$m. The communication topology and desired formation of UAVs are shown in Figure 20(a). For simplicity, we only consider the impact of time delay on formation. As shown in Figure 20(b), the UAVs cannot converge to the desired formation in a short time subject to time delay. The result is similar to [38], which indicates that this objective is difficult to achieve if the communication uncertainties are not compensated for elaborately in formation controllers.

Estimating-and-then-compensating is a way to deal with uncertainty. However, a deadlock may happen if the noise, delay, or packet loss is not compensated elaborately. Let us consider a simple but particular example that two UAVs pass through a trapezoid tube. As shown in Figure 21(a), in the presence of uncertainties, UAV1 considers UAV2 at the position of UAV2', while UAV2 considers UAV1 at the position of UAV1'. In this case, a deadlock will exist, namely, each UAV cannot pass the exit. Even if a deadlock does not exist, these uncertainties will slow down the movement of the swarm. The proposed safety radius for uncertainties can solve this problem by separating the two UAVs large enough as shown in Figure 21(b). However, a big safety radius will decrease traffic efficiency, but, on the other hand, make sure safety. A further study on safety radius is deserved to achieve a trade-off between safety and efficiency for UAV swarm.

2) Calculation Speed Analysis of Optimal Trajectory Method & Forcefield-Based Method with Safety Radius Design: We discuss the performance of different control methods with the safety radius design. The objective of the optimal trajectory method requires optimal solutions of length, time, or energy of path, which leads to longer calculation time of the online path-planning problem. In the simulation, we compare the online path-planning calculation speed of an optimization-based algorithm with the forcefield-based method by MATLAB. In [39], a path-planning algorithm using Bezier curves with the open-source code at https://github.com/byuflowlab/uav-path-optimization is proposed, which can find the optimal solutions to the offline and online path-planning problem. We design a scenario that contains 10 UAVs at the same altitude with $r_{\mathrm{s}} = 5$m. The initial position of 1st UAV $\mathbf{p}_1(0) = [0\ 0\ 100]^{\mathrm{T}}$m, while the other UAVs are distributed

randomly in a 100m $\times$ 100m space with a constant velocity $[1\ 0\ 0]^{\mathrm{T}}$. For two different algorithms, we design 10 sets of random initial positions for the other UAVs, run the simulation on the same computer, and record the *average calculation time* when the 1st UAV get a feasible path to its destination $[100\ 0\ 100]^{\mathrm{T}}$m. Figure 22 shows the calculation speed performance with respect to the density by changing the safety radius and the number of UAVs separately. As shown in Figure 22, for the same airspace, if the number of UAVs increases or the safety radius of UAVs gets larger, the calculation speed of the optimization-based algorithm will be decreased rapidly because the probability of constraint being triggered is increasing, which brings more complex calculations. On the contrary, the forcefield-based method can better deal with such an online path-planning problem. However, the optimal trajectory method is better to deal with the offline path-planning problem.

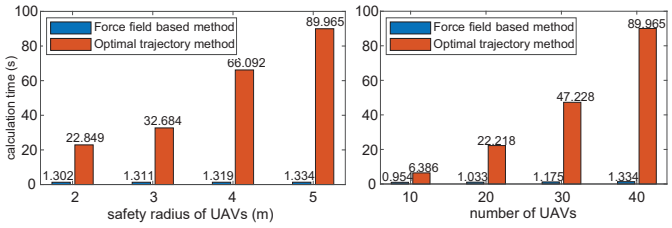

Fig. 22. Calculation speed of different algorithms.

VI. Conclusions

How to decide the safety radius taking communication uncertainties into consideration is studied in this paper. First, a VTOL UAV model and obstacle model are introduced. Then, some assumptions of communication and control are made, including estimated noise, broadcast delay, and packet loss. Based on models and assumptions, problems are formulated to determine the designed safety radius in the design phase objective and the practical safety radius in the flight phase objective. For the first objective, the principle of separation of control and safety radius (*Theorem 1*) is proposed. With this principle, the designed safety radius is determined in *Theorems 2,4*. Then, the practical safety radius is determined in *Theorems 3,5*. By the proposed methods, a UAV can keep a safe distance from other obstacles during the whole flight. This is very necessary to guarantee flight safety in practice. Simulations and experiments are given to show the effectiveness of the proposed method from the functional requirement and the safety requirement.

VII. Appendix

A. Proof of Lemma 1

(i) *Proof of Sufficiency*. Since

$$\dot{\tilde{\boldsymbol{\xi}}}_{\mathrm{o}} = \mathbf{c}\left(t, \tilde{\boldsymbol{\xi}}_{\mathrm{o}}\right) - \dot{\boldsymbol{\xi}}_{\mathrm{o}}$$

we have

$$\tilde{\boldsymbol{\xi}}_{\mathrm{o}}^{\mathrm{T}} \dot{\tilde{\boldsymbol{\xi}}}_{\mathrm{o}} = \tilde{\boldsymbol{\xi}}_{\mathrm{o}}^{\mathrm{T}}\left(\mathbf{c}\left(t, \tilde{\boldsymbol{\xi}}_{\mathrm{o}}\right) - \dot{\boldsymbol{\xi}}_{\mathrm{o}}\right). \tag{45}$$

If (17) is violated, due to the continuity of $\tilde{\boldsymbol{\xi}}_{\mathrm{o}}$, there must exist a time $t = t_1$ such that $\left\|\tilde{\boldsymbol{\xi}}_{\mathrm{o}}^{\mathrm{T}}(t_1)\,\tilde{\boldsymbol{\xi}}_{\mathrm{o}}(t_1)\right\| = (r_{\mathrm{s}} + r_{\mathrm{o}})^2$. Since $\left\|\dot{\boldsymbol{\xi}}_{\mathrm{o}}\right\| \le v_{\mathrm{m}}$, (45) becomes

$$\begin{aligned}\tilde{\boldsymbol{\xi}}_{\mathrm{o}}^{\mathrm{T}} \dot{\tilde{\boldsymbol{\xi}}}_{\mathrm{o}}\Big|_{t=t_1} &\ge \tilde{\boldsymbol{\xi}}_{\mathrm{o}}^{\mathrm{T}}\mathbf{c}\left(t_1, \tilde{\boldsymbol{\xi}}_{\mathrm{o}}\right) - \left\|\tilde{\boldsymbol{\xi}}_{\mathrm{o}}(t_1)\right\|\left\|\dot{\boldsymbol{\xi}}_{\mathrm{o}}(t_1)\right\| \\ &\ge \tilde{\boldsymbol{\xi}}_{\mathrm{o}}^{\mathrm{T}}\mathbf{c}\left(t_1, \tilde{\boldsymbol{\xi}}_{\mathrm{o}}\right) - (r_{\mathrm{s}} + r_{\mathrm{o}})\, v_{\mathrm{m}}.\end{aligned}$$

If (18) holds, then $\tilde{\boldsymbol{\xi}}_{\mathrm{o}}^{\mathrm{T}} \dot{\tilde{\boldsymbol{\xi}}}_{\mathrm{o}}\Big|_{t=t_1} \ge 0$. This implies that $\left\|\tilde{\boldsymbol{\xi}}_{\mathrm{o}}^{\mathrm{T}}(t_1)\,\tilde{\boldsymbol{\xi}}_{\mathrm{o}}(t_1)\right\|$ will not be decreased any more. So, (17) cannot be violated for any $\left\|\tilde{\boldsymbol{\xi}}_{\mathrm{o}}(0)\right\| \ge r_{\mathrm{s}} + r_{\mathrm{o}}$. (ii) *Proof of Necessity*. This necessary condition is proved by contradiction. Suppose that there exists an $\mathbf{x}^* \in \mathcal{C}$ such that

$$\begin{aligned}\mathbf{x}^{*\mathrm{T}}\mathbf{c}(t, \mathbf{x}^*) &= (r_{\mathrm{s}} + r_{\mathrm{o}})\, v_{\mathrm{m}} - \epsilon \\ &< (r_{\mathrm{s}} + r_{\mathrm{o}})\, v_{\mathrm{m}}\end{aligned}$$

where $\epsilon > 0$. We will show that (17) will not hold for any obstacle $\left\|\dot{\boldsymbol{\xi}}_{\mathrm{o}}\right\| \le v_{\mathrm{m}}$ and $\left\|\tilde{\boldsymbol{\xi}}_{\mathrm{o}}(0)\right\| \ge r_{\mathrm{s}} + r_{\mathrm{o}}$. Let $\tilde{\boldsymbol{\xi}}_{\mathrm{o}}(0) = \mathbf{x}^*$ and

$$\dot{\boldsymbol{\xi}}_{\mathrm{o}}(0) = \frac{v_{\mathrm{m}}}{r_{\mathrm{s}} + r_{\mathrm{o}}}\tilde{\boldsymbol{\xi}}_{\mathrm{o}}(0).$$

So, $\left\|\dot{\boldsymbol{\xi}}_{\mathrm{o}}(0)\right\| = \frac{v_{\mathrm{m}}}{r_{\mathrm{s}}+r_{\mathrm{o}}}\left\|\tilde{\boldsymbol{\xi}}_{\mathrm{o}}(0)\right\| = v_{\mathrm{m}}$. In this case, (45) becomes

$$\begin{aligned}\tilde{\boldsymbol{\xi}}_{\mathrm{o}}^{\mathrm{T}} \dot{\tilde{\boldsymbol{\xi}}}_{\mathrm{o}}\Big|_{t=0} &= (r_{\mathrm{s}} + r_{\mathrm{o}})\, v_{\mathrm{m}} - \epsilon - \frac{v_{\mathrm{m}}}{r_{\mathrm{s}} + r_{\mathrm{o}}}\tilde{\boldsymbol{\xi}}_{\mathrm{o}}^{\mathrm{T}}(0)\,\tilde{\boldsymbol{\xi}}_{\mathrm{o}}(0) \\ &= -\epsilon < 0.\end{aligned}$$

This implies that $\left\|\tilde{\boldsymbol{\xi}}_{\mathrm{o}}(t)\right\|$ will be further decreased around $t = 0$, namely there exists a $t = t_2$ such that $\left\|\tilde{\boldsymbol{\xi}}_{\mathrm{o}}(t_2)\right\| < r_{\mathrm{s}} + r_{\mathrm{o}}$. This contradicts with (17). So, (18) is also necessary. □

B. Proof of Lemma 2

First, multiplying $\mathbf{x}^{\mathrm{T}}(t)$ on the left side of (24) results in

$$\mathbf{x}^{\mathrm{T}}(t)\,\dot{\mathbf{x}}(t) = -k(t)\,\mathbf{x}^{\mathrm{T}}(t)\,\mathbf{x}(t) + k(t)\,\mathbf{x}^{\mathrm{T}}(t)\,\mathbf{y}(t). \tag{46}$$

Since

$$\begin{aligned}\mathbf{x}^{\mathrm{T}}(t)\,\dot{\mathbf{x}}(t) &= \frac{1}{2}\frac{\mathrm{d}\mathbf{x}^{\mathrm{T}}(t)\,\mathbf{x}(t)}{\mathrm{d}t} \\ &= \frac{1}{2}\frac{\mathrm{d}\left\|\mathbf{x}(t)\right\|^2}{\mathrm{d}t} = \left\|\mathbf{x}(t)\right\|\frac{\mathrm{d}\left\|\mathbf{x}(t)\right\|}{\mathrm{d}t}\end{aligned} \tag{47}$$

the equation (46) becomes

$$\frac{\mathrm{d}\left\|\mathbf{x}(t)\right\|}{\mathrm{d}t} = -k(t)\left\|\mathbf{x}(t)\right\| + k(t)\,\frac{1}{\left\|\mathbf{x}(t)\right\|}\mathbf{x}^{\mathrm{T}}(t)\,\mathbf{y}(t).$$

If $\left\|\mathbf{y}(t)\right\| \le y_{\max}$, then

$$\frac{\mathrm{d}\left\|\mathbf{x}(t)\right\|}{\mathrm{d}t} \le -k(t)\left\|\mathbf{x}(t)\right\| + k(t)\,y_{\max}.$$

Let $z \triangleq \|\mathbf{x}\| - y_{\max}$. Then

$$\frac{\mathrm{d}z(t)}{\mathrm{d}t} \le -k(t)\,z(t).$$

We consider another equation that

$$\frac{\mathrm{d}z'(t)}{\mathrm{d}t} = -k(t)\, z'(t), z'(0) = z(0).$$

The solution to the equation above is

$$z'(t) = e^{\int_0^t -k(s)\mathrm{d}s} z(0). \tag{48}$$

Since $z(0) \leq 0$, we have $z'(t) \leq 0$ according to (48). Consequently, $z(t) \leq z'(t) \leq 0$ according to the comparison lemma [40, p. 102], namely $\|\mathbf{x}(t)\| \leq y_{\max}$.

In the following, the conclusion (26) will be shown. Let $\mathbf{z} \triangleq \mathbf{x} - \mathbf{y}$. Then (24) can be transformed as

$$\dot{\mathbf{z}}(t) = -k(t)\,\mathbf{z}(t) + k(t)\left(\frac{1}{k(t)}\dot{\mathbf{y}}\right).$$

If $\|\mathbf{z}(0)\| \leq \frac{1}{k_{\min}} v_{y_{\max}}$, then

$$\|\mathbf{z}(t)\| \leq \frac{1}{k_{\min}} v_{y_{\max}} \tag{49}$$

where the conclusion (25) is utilized. The equation (24) is further written as

$$\dot{\mathbf{x}}(t) = -k(t)\,\mathbf{z}(t).$$

It can be further written as

$$\begin{aligned}\|\dot{\mathbf{x}}(t)\| &\leq |k(t)|\,\|\mathbf{z}(t)\| \\ &\leq k_{\max}\|\mathbf{z}(t)\|.\end{aligned}$$

Using (49) will lead to the conclusion (26). □

C. Proof of Proposition 2

(i) Proof of sufficiency. Let

$$\begin{aligned}p &= \tilde{\mathbf{p}}_{\mathrm{o}}^{\mathrm{T}}\tilde{\mathbf{p}}_{\mathrm{o}} \\ \delta &= \tilde{\boldsymbol{\xi}}_{\mathrm{o}}^{\mathrm{T}}\tilde{\boldsymbol{\xi}}_{\mathrm{o}} - \frac{1}{l^2}\tilde{\mathbf{v}}_{\mathrm{o}}^{\mathrm{T}}\tilde{\mathbf{v}}_{\mathrm{o}}.\end{aligned}$$

According to (14), we have

$$\begin{aligned}\tilde{\boldsymbol{\xi}}_{\mathrm{o}}^{\mathrm{T}}\tilde{\boldsymbol{\xi}}_{\mathrm{o}} &= \left(\tilde{\mathbf{p}}_{\mathrm{o}} + \frac{1}{l}\tilde{\mathbf{v}}_{\mathrm{o}}\right)^{\mathrm{T}}\left(\tilde{\mathbf{p}}_{\mathrm{o}} + \frac{1}{l}\tilde{\mathbf{v}}_{\mathrm{o}}\right) \\ &= \tilde{\mathbf{p}}_{\mathrm{o}}^{\mathrm{T}}\tilde{\mathbf{p}}_{\mathrm{o}} + \frac{1}{l^2}\tilde{\mathbf{v}}_{\mathrm{o}}^{\mathrm{T}}\tilde{\mathbf{v}}_{\mathrm{o}} + \frac{2}{l}\tilde{\mathbf{v}}_{\mathrm{o}}^{\mathrm{T}}\tilde{\mathbf{p}}_{\mathrm{o}}.\end{aligned} \tag{50}$$

Since

$$\dot{p} = 2\tilde{\mathbf{p}}_{\mathrm{o}}^{\mathrm{T}}\tilde{\mathbf{v}}_{\mathrm{o}}$$

using the equation (50), we further have

$$\dot{p} = -lp + l\delta. \tag{51}$$

The solution $p(t)$ can be expressed as

$$p(t) = e^{-lt}p(0) + \int_0^t e^{-l(t-s)} l\delta(s)\,\mathrm{d}s. \tag{52}$$

With (27) in hand, if condition (29) is satisfied, then

$$\delta(t) = \tilde{\boldsymbol{\xi}}_{\mathrm{o}}^{\mathrm{T}}\tilde{\boldsymbol{\xi}}_{\mathrm{o}} - \frac{1}{l^2}\tilde{\mathbf{v}}_{\mathrm{o}}^{\mathrm{T}}\tilde{\mathbf{v}}_{\mathrm{o}} \geq r^2.$$

Since $\|\tilde{\mathbf{p}}_{\mathrm{o}}(0)\| > r$, we have $p(0) > r^2$. The solution in (52) satisfies

$$\begin{aligned}p(t) &\geq e^{-lt}r^2 + r^2\int_0^t e^{-l(t-s)} l\mathrm{d}s \\ &= r^2.\end{aligned}$$

Based on it, we have $\|\tilde{\mathbf{p}}_{\mathrm{o}}(t)\| \geq r$, where $t \geq 0$. If $\frac{\mathbf{v}^{\mathrm{T}}\mathbf{v}_{\mathrm{o}}}{\|\mathbf{v}\|\|\mathbf{v}_{\mathrm{o}}\|} = -1$, then the UAV and the obstacle are in the case shown in Figure 2(b). Thus,

$$\frac{1}{l^2}\tilde{\mathbf{v}}_{\mathrm{o}}^{\mathrm{T}}\tilde{\mathbf{v}}_{\mathrm{o}} = r_{\mathrm{v}}^2.$$

Consequently, $\delta(t) = r^2$. Furthermore, if $\left\|\tilde{\boldsymbol{\xi}}_{\mathrm{o}}(t)\right\| > \sqrt{r^2 + r_{\mathrm{v}}^2}$ and $\|\tilde{\mathbf{p}}_{\mathrm{o}}(0)\| > r$, then $\|\tilde{\mathbf{p}}_{\mathrm{o}}(t)\| > r$, where $t > 0$.

(ii) Proof of necessity. Given any $\epsilon_{\mathrm{o}} > 0$, we will show if

$$\left\|\tilde{\boldsymbol{\xi}}_{\mathrm{o}}(t)\right\|^2 = r^2 + r_{\mathrm{v}}^2 - \epsilon_{\mathrm{o}},$$

and $\|\tilde{\mathbf{p}}_{\mathrm{o}}(0)\| = r$, then there exists a case that $\|\tilde{\mathbf{p}}_{\mathrm{o}}(t)\| < r$, where $t \geq 0$. Consider a case $\frac{\mathbf{v}^{\mathrm{T}}\mathbf{v}_{\mathrm{o}}}{\|\mathbf{v}\|\|\mathbf{v}_{\mathrm{o}}\|} = -1$. Then the UAV and the obstacle are in the case shown in Figure 2(b). Thus,

$$\delta(t) = \tilde{\boldsymbol{\xi}}_{\mathrm{o}}^{\mathrm{T}}\tilde{\boldsymbol{\xi}}_{\mathrm{o}} - \frac{1}{l^2}\tilde{\mathbf{v}}_{\mathrm{o}}^{\mathrm{T}}\tilde{\mathbf{v}}_{\mathrm{o}} = r^2 - \epsilon_{\mathrm{o}}.$$

According to (52), we have

$$\begin{aligned}p(t) &= r^2 - \int_0^t e^{-l(t-s)} l\epsilon_{\mathrm{o}}\mathrm{d}s \\ &< r^2.\end{aligned}$$

Therefore, $\|\tilde{\mathbf{p}}_{\mathrm{o}}(t)\| < r$, where $t \geq 0$. □

D. Proof of Theorem 1

Proof of Conclusion (i). According to (19) in the proof of *Lemma 1*, if and only if

$$\mathbf{e}_{\mathrm{o}}^{\mathrm{T}}\dot{\mathbf{e}}_{\mathrm{o}}\big|_{\|\mathbf{e}_{\mathrm{o}}\| = r_{\mathrm{s}} + r_{\mathrm{o}}} \geq 0 \tag{53}$$

then (23) holds with $\hat{r}_{\mathrm{s}} = r_{\mathrm{s}}$ for any $\|\mathbf{e}_{\mathrm{o}}(0)\| \geq r_{\mathrm{s}} + r_{\mathrm{o}}$. The derivative of $\mathbf{e}_{\mathrm{o}}$ is

$$\dot{\mathbf{e}}_{\mathrm{o}} = \dot{\boldsymbol{\xi}} - \dot{\tilde{\boldsymbol{\xi}}}_{\mathrm{o}} + \dot{\boldsymbol{\varepsilon}}.$$

Then, the inequality (53) is rewritten as

$$\left(\mathbf{e}_{\mathrm{o}}^{\mathrm{T}}\dot{\boldsymbol{\xi}} - \mathbf{e}_{\mathrm{o}}^{\mathrm{T}}\dot{\tilde{\boldsymbol{\xi}}}_{\mathrm{o}} + \mathbf{e}_{\mathrm{o}}^{\mathrm{T}}\dot{\boldsymbol{\varepsilon}}\right)\Big|_{\|\mathbf{e}_{\mathrm{o}}\| = r_{\mathrm{s}} + r_{\mathrm{o}}} \geq 0. \tag{54}$$

i) *Proof of Sufficiency*. Since $\|\dot{\boldsymbol{\varepsilon}}\| \leq v_b$, we have

$$\begin{aligned}&\left(\mathbf{e}_{\mathrm{o}}^{\mathrm{T}}\dot{\boldsymbol{\xi}} - \mathbf{e}_{\mathrm{o}}^{\mathrm{T}}\dot{\tilde{\boldsymbol{\xi}}}_{\mathrm{o}} + \mathbf{e}_{\mathrm{o}}^{\mathrm{T}}\dot{\boldsymbol{\varepsilon}}\right)\Big|_{\|\mathbf{e}_{\mathrm{o}}\| = r_{\mathrm{s}} + r_{\mathrm{o}}} \\ \geq\ &\left(\mathbf{e}_{\mathrm{o}}^{\mathrm{T}}\dot{\boldsymbol{\xi}} - \mathbf{e}_{\mathrm{o}}^{\mathrm{T}}\dot{\tilde{\boldsymbol{\xi}}}_{\mathrm{o}} - \|\mathbf{e}_{\mathrm{o}}\|\,\|\dot{\boldsymbol{\varepsilon}}\|\right)\Big|_{\|\mathbf{e}_{\mathrm{o}}\| = r_{\mathrm{s}} + r_{\mathrm{o}}} \\ \geq\ &\left(\mathbf{e}_{\mathrm{o}}^{\mathrm{T}}\dot{\boldsymbol{\xi}} - \mathbf{e}_{\mathrm{o}}^{\mathrm{T}}\dot{\tilde{\boldsymbol{\xi}}}_{\mathrm{o}}\right)\Big|_{\|\mathbf{e}_{\mathrm{o}}\| = r_{\mathrm{s}} + r_{\mathrm{o}}} - (r_{\mathrm{s}} + r_{\mathrm{o}})\, v_b.\end{aligned}$$

Therefore, if (30) holds, then (54) is satisfied.

ii) *Proof of Necessity*. The necessary condition is proved by contradiction. Suppose (30) is not satisfied, namely there exists an $\mathbf{e}_{\mathrm{o}}^*$ with $\epsilon > 0$ such that

$$\left(\mathbf{e}_{\mathrm{o}}^{*\mathrm{T}}\dot{\boldsymbol{\xi}} - \mathbf{e}_{\mathrm{o}}^{*\mathrm{T}}\dot{\tilde{\boldsymbol{\xi}}}_{\mathrm{o}}\right)\Big|_{\|\mathbf{e}_{\mathrm{o}}^*\| = r_{\mathrm{s}} + r_{\mathrm{o}}} = (r_{\mathrm{s}} + r_{\mathrm{o}})\, v_b - \epsilon.$$

Then, choose $\dot{\boldsymbol{\varepsilon}} = -v_b \frac{\mathbf{e}_\mathrm{o}^*}{r_\mathrm{s}+r_\mathrm{o}}$ when $\mathbf{e}_\mathrm{o} = \mathbf{e}_\mathrm{o}^*$, which satisfies $\|\dot{\boldsymbol{\varepsilon}}\| \leq v_b$. As a result, at $\mathbf{e}_\mathrm{o} = \mathbf{e}_\mathrm{o}^*$, (54) becomes

$$(r_\mathrm{s}+r_\mathrm{o})\, v_b - \epsilon - v_b \mathbf{e}_\mathrm{o}^{*\mathrm{T}} \frac{\mathbf{e}_\mathrm{o}^*}{r_\mathrm{s}+r_\mathrm{o}} \geq 0$$

namely,

$$-\epsilon \geq 0.$$

This is a contradiction. This is implies that (54) and then (53) will be violated.

Proof of Conclusion (ii). Under *Assumption 3*, according to *Lemma 1*, we have

$$\mathbf{e}_\mathrm{o}^\mathrm{T} \mathbf{c}\left(t, \mathbf{e}_\mathrm{o}\right)\big|_{\|\mathbf{e}_\mathrm{o}\|=r_\mathrm{s}+r_\mathrm{o}} \geq (r_\mathrm{s}+r_\mathrm{o})\, v_\mathrm{m}. \tag{55}$$

Therefore, (30) becomes (31).

Proof of Conclusion (iii). In view of (9), according to *Lemma 2*, we have

$$\left\|\dot{\tilde{\boldsymbol{\xi}}}_\mathrm{o}\right\| \leq \left\|\dot{\boldsymbol{\xi}}_\mathrm{o}\left(t-\tau_\mathrm{d}\right)\right\| \leq v_\mathrm{o}.$$

Then

$$\begin{aligned}\mathbf{e}_\mathrm{o}^\mathrm{T}\dot{\tilde{\boldsymbol{\xi}}}_\mathrm{o}\Big|_{\|\mathbf{e}_\mathrm{o}\|=r_\mathrm{s}+r_\mathrm{o}} &\leq \left(\|\mathbf{e}_\mathrm{o}\|\left\|\dot{\tilde{\boldsymbol{\xi}}}_\mathrm{o}\right\| + \|\mathbf{e}_\mathrm{o}\|\,\|\boldsymbol{\varepsilon}_\mathrm{o}\|\right)_{\|\mathbf{e}_\mathrm{o}\|=r_\mathrm{s}+r_\mathrm{o}} \\ &\leq (r_\mathrm{s}+r_\mathrm{o})\left(v_\mathrm{o}+v_{b_\mathrm{o}}\right).\end{aligned}$$

If (32) holds, then (31) holds. Therefore, (23) holds with $\hat{r}_\mathrm{s} = r_\mathrm{s}$. □

E. Proof of Proposition 3

Since $\mathbf{e}_\mathrm{o}$ in (21) can be written as

$$\mathbf{e}_\mathrm{o} = \tilde{\boldsymbol{\xi}}_\mathrm{o} + (\boldsymbol{\lambda}_\mathrm{o} - \boldsymbol{\varepsilon}_\mathrm{o} + \boldsymbol{\varepsilon}) \tag{56}$$

where

$$\boldsymbol{\lambda}_\mathrm{o} \triangleq \boldsymbol{\xi}_\mathrm{o} - \bar{\boldsymbol{\xi}}_\mathrm{o}.$$

Taking the norm on both sides of (56) results in

$$\|\mathbf{e}_\mathrm{o}\| \leq \left\|\tilde{\boldsymbol{\xi}}_\mathrm{o}\right\| + \|\boldsymbol{\lambda}_\mathrm{o}\| + \|\boldsymbol{\varepsilon}_\mathrm{o}\| + \|\boldsymbol{\varepsilon}\|.$$

If (34) holds, then

$$\begin{aligned}\left\|\tilde{\boldsymbol{\xi}}_\mathrm{o}\left(t\right)\right\| &\geq r + r_e - \left(\|\boldsymbol{\lambda}_\mathrm{o}\| + \|\boldsymbol{\varepsilon}_\mathrm{o}\| + \|\boldsymbol{\varepsilon}\|\right) \\ &\geq r + \frac{\theta_\mathrm{m} T_\mathrm{s}}{1-\theta_\mathrm{m}} v_\mathrm{o} + v_\mathrm{o}\tau_\mathrm{dm} - \|\boldsymbol{\lambda}_\mathrm{o}\|\end{aligned} \tag{57}$$

where *Assumptions 1-2* are utilized. The left work is to study $\|\boldsymbol{\lambda}_\mathrm{o}\|$. The derivative of $\boldsymbol{\lambda}_\mathrm{o}$ is

$$\begin{aligned}\dot{\boldsymbol{\lambda}}_\mathrm{o}\left(t\right) &= \dot{\boldsymbol{\xi}}_\mathrm{o}\left(t\right) + \frac{1-\theta}{\theta T_\mathrm{s}}\bar{\boldsymbol{\xi}}_\mathrm{o}\left(t\right) - \frac{1-\theta}{\theta T_\mathrm{s}}\boldsymbol{\xi}_\mathrm{o}\left(t-\tau_\mathrm{d}\right) \\ &= -\frac{1-\theta}{\theta T_\mathrm{s}}\boldsymbol{\lambda}_\mathrm{o}\left(t\right) \\ &\quad + \frac{1-\theta}{\theta T_\mathrm{s}}\left(\left(\boldsymbol{\xi}_\mathrm{o}\left(t\right) - \boldsymbol{\xi}_\mathrm{o}\left(t-\tau_\mathrm{d}\right)\right) + \frac{\theta T_\mathrm{s}}{1-\theta}\dot{\boldsymbol{\xi}}_\mathrm{o}\left(t\right)\right).\end{aligned} \tag{58}$$

As for term $\boldsymbol{\xi}_\mathrm{o}\left(t\right) - \boldsymbol{\xi}_\mathrm{o}\left(t-\tau_\mathrm{d}\right)$, by the mean value theorem, we have

$$\boldsymbol{\xi}_\mathrm{o}\left(t\right) - \boldsymbol{\xi}_\mathrm{o}\left(t-\tau_\mathrm{d}\right) = \dot{\boldsymbol{\xi}}_\mathrm{o}\left(st + (1-s)\left(t-\tau_\mathrm{d}\right)\right)\tau_\mathrm{d},\ \ s \in [0,1].$$

Then

$$\left\|\boldsymbol{\xi}_\mathrm{o}\left(t-\tau_\mathrm{d}\right) - \boldsymbol{\xi}_\mathrm{o}\left(t\right)\right\| \leq v_\mathrm{o}\tau_\mathrm{d}$$

where $\max\left\|\dot{\boldsymbol{\xi}}_\mathrm{o}\right\| \leq v_\mathrm{o}$ is utilized. Similarly, $\|\boldsymbol{\lambda}_\mathrm{o}\left(0\right)\| \leq v_\mathrm{o}\tau_\mathrm{d}$ by *Assumption 2*. Furthermore, based on the equation (58), according to *Lemma 2*, we have

$$\begin{aligned}\|\boldsymbol{\lambda}_\mathrm{o}\left(t\right)\| &\leq v_\mathrm{o}\tau_\mathrm{d} + \frac{\theta T_\mathrm{s}}{1-\theta} v_\mathrm{o} \\ &\leq v_\mathrm{o}\tau_\mathrm{dm} + \frac{\theta_\mathrm{m} T_\mathrm{s}}{1-\theta_\mathrm{m}} v_\mathrm{o}.\end{aligned} \tag{59}$$

Using (57) and (59) yields (35). □

REFERENCES

[1] K. Balakrishnan, J. Polastre, J. Mooberry, R. Golding, P. Sachs, "Premiering a future blueprint for our sky"[online], Available:https://storage.googleapis.com/blueprint/Airbus_UTM_Blueprint.pdf

[2] NASA, "UAS traffic management (UTM)"[online], Available:https://utm.arc.nasa.gov

[3] SESAR, "European drones outlook 2016"[online], Available:https://www.sesarju.eu/sites/default/files/documents/reports/European_Drones_Outlook_Study_2016.pdf

[4] D. Depoorter and W. Kellerer, "Designing the Air–Ground Data Links for Future Air Traffic Control Communications", *IEEE Transactions on Aerospace and Electronic Systems*, vol. 55, no. 1, pp. 135-146, 2019.

[5] RTCA, "Final report of the RTCA task force 3, free flight implementation", Washington, DC:RTCA, Inc., 1995.

[6] J. Kosecka, C. Tomlin, G. Pappas, S. Sastry, "Generation of conflict resolution manoeuvres for air traffic management", *1997 IEEE/RSJ International Conference on Intelligent Robot and Systems*, Grenoble, France, vol. 3, pp. 1598-1603, 1997.

[7] ICAO, "The use of displayed ADS-B data for a collision avoidance capability in unmanned aircraft system", UASSG/9-SN, no. 5, 2012.

[8] A. Chakrabarty, C.A. Ippolito, J. Baculi, K.S. Krishnakumar, S. Hening, "Vehicle to vehicle (V2V) communication for collision avoidance for multicopters flying in UTM-TCL4", *AIAA Scitech 2019 Forum*, San Diego, California, AIAA 2019-0690, 2019.

[9] S. Hayat, E. Yanmaz, R. Muzaffar, "Survey on unmanned aerial vehicle networks for civil applications: a communications viewpoint", *IEEE Communications Surveys & Tutorials*, vol. 18, no. 4, pp. 2624-2661, 2016.

[10] GSMA, "Mobile-enabled unmanned aircraft"[online], Available:https://www.gsma.com/iot/wp-content/uploads/2018/02/Mobile-Enabled-Unmanned-Aircraft-web.pdf

[11] R. Dutta, L. Sun, D. Pack, "A decentralized formation and network connectivity tracking controller for multiple unmanned systems", *IEEE Transactions on Control Systems Technology*, vol. 26, no. 6, pp. 2206-2213, 2018.

[12] L.J. Glaab, C.V. Dolph, S.D. Young, N.C. Coffey, R.G. McSwain, M.J. Logan, D.E. Harper, "Small unmanned aerial system (UAS) flight testing of enabling vehicle technologies for the UAS traffic management project", NASA/TM–2018-219816, 2018.

[13] E.J. Rodríguez-Seda, D.M. Stipanović, M.W. Spong, "Guaranteed collision avoidance for autonomous systems with acceleration constraints and sensing uncertainties", *Journal of Optimization Theory and Applications*, vol. 168, no. 3, pp. 1014-1038, 2016.

[14] S. Huang, R.S.H. Teo, K.K. Tan, "Collision avoidance of multi unmanned aerial vehicles: a review", *Annual Reviews in Control*, vol. 48, pp. 147-164, 2019.

[15] Y. Lin and S. Saripalli, "Sampling-based path planning for UAV collision avoidance", *IEEE Transactions on Intelligent Transportation Systems*, vol. 18, no. 11, pp. 3179–3192, 2017.

[16] Y. I. Jenie, E.-J. van Kampen, J. Ellerbroek, J. M. Hoekstra, "Taxonomy of conflict detection and resolution approaches for unmanned aerial vehicle in an integrated airspace", *IEEE Transactions on Intelligent Transportation Systems*, vol. 18, no. 3, pp. 558–567, 2017.

[17] Y. Rasekhipour, A. Khajepour, S.-K. Chen, and B. Litkouhi, "A potential field-based model predictive path-planning controller for autonomous road vehicles", *IEEE Transactions on Intelligent Transportation Systems*, vol. 18, no. 5, pp. 1255–1267, May 2017.

[18] J. Van Den Berg, S. J. Guy, M. Lin, D. Manocha, "Reciprocal n-body collision avoidance", in *Robotics Research*, Berlin, Germany:Springer, pp. 3-19, 2011.

[19] A. Alonso-Ayuso, S. F. Escudero, F. J. Martin-Campo, "Collision avoidance in air traffic management: A mixed-integer linear optimization approach", *IEEE Transactions on Intelligent Transportation Systems*, vol. 12, no. 1, pp. 47–57, 2011.

[20] Q. Quan, R. Fu, K-Y. Cai, "Practical control for multicopters to avoid non-cooperative moving obstacles," *IEEE Transactions on Intelligent Transportation Systems*, doi: 10.1109/TITS.2021.3096558. (early access)

[21] E. Mueller and M. J. Kochenderfer, "Simulation comparison of collision avoidance algorithms for small multi-rotor aircraft", *AIAA Modeling and Simulation Technologies Conference*, Washington, D.C., AIAA-2016-3674, 2016.

[22] H. Bai, D. Hsu, M.J. Kochenderfer, W.S. Lee, "Unmanned aircraft collision avoidance using continuous-state POMDPs", *Proceedings of Robotics: Science and Systems*, Los Angeles, CA, Bai-RSS-11, 2011.

[23] H. Yang, J. Lim, S. Yoon, "Anytime RRBT for handling uncertainty and dynamic objects", *2016 IEEE/RSJ International Conference on Intelligent Robots and Systems (IROS)*, Daejeon, pp. 4786-4793, 2016.

[24] S.H. Arul, A.J. Sathyamoorthy, S. Patel, M. Otte, H. Xu, M.C. Lin, and D. Manocha, "LSwarm: efficient collision avoidance for large swarms with coverage constraints in complex urban scenes", *IEEE Robotics and Automation Letters*, vol. 4, no. 4, pp. 3940-3947, 2019.

[25] G. Angeris, K. Shah, M. Schwager, "Fast reciprocal collision avoidance under measurement uncertainty", arXiv preprint arXiv:1905.12875, 2019.

[26] J. Alonso-Mora, P. Beardsley, R. Siegwart, "Cooperative collision avoidance for nonholonomic robots", *IEEE Transactions on Robotics*, vol. 34, no. 2, pp. 404-420, 2018.

[27] M.H. Yamchi, R.M. Esfanjani. "Distributed predictive formation control of networked mobile robots subject to communication delay", *Robotics and Autonomous Systems*, vol. 91, pp. 194-207, 2017.

[28] C. Virágh, M. Nagy, C. Gershenson, G. Vásárhelyi, "Self-organized UAV traffic in realistic environments", *2016 IEEE/RSJ International Conference on Intelligent Robots and Systems (IROS)*, Daejeon, pp. 1645-1652, 2016.

[29] J. Hoekstra, R. van Gent, R. Ruigrok, "Conceptual design of free flight with airborne separation assurance", *Navigation, and Control Conference and Exhibit*, Boston, MA, AIAA-98-4239, 1998.

[30] S. M. Iranmanesh, E. Moradi-Pari, Y.P. Fallah, S. Das, M. Rizwan, "Robustness of cooperative forward collision warning systems to communication uncertainty", *2016 Annual IEEE Systems Conference (SysCon)*, Orlando, FL, pp. 1-7, 2016.

[31] M. Gharibi, R. Boutaba, S.L. Waslander, "Internet of drones", *IEEE Access*, vol. 4, pp. 1148-1162, 2016.

[32] P. Menon, "Short-range nonlinear feedback strategies for aircraft pursuit-evasion," *Journal of Guidance, Control, and Dynamics*, vol. 12, no. 1, pp. 27–32, 1989.

[33] D. Trany, D. Casbeery, E. Garciay, I. E. Weintrauby, D. Milutinović, "Ring Formation Maneuvering with Double Integrator Dynamics", *2021 International Conference on Unmanned Aircraft Systems (ICUAS)*, Athens, 2021, pp. 1580-1586.

[34] R. Vidal, O. Shakernia, H.J. Kim, D.H. Shim, S. Sastry, "Probabilistic pursuit-evasion games: theory, implementation, and experimental evaluation", *IEEE Transactions on Robotics and Automation*, vol. 18, no. 5, pp. 662-669, 2002.

[35] A. Kamimura and T. Ohira, "Group chase and escape", *New Journal of Physics*, vol. 12, pp. 1-13, 2010.

[36] R. Fu, Q. Quan, M. Li, K-Y. Cai, "Practical distributed control for cooperative multicopters in structured free flight concepts", arXiv preprint arXiv:2111.11049, 2021.

[37] K. Oh, M. Park, H. Ahn, "A survey of multi-agent formation control", *Automatica*, 2015.

[38] R. Olfati-Saber and R. M. Murray, "Consensus problems in networks of agents with switching topology and time-delays", *IEEE Transactions on Automatic Control*, vol. 49, no. 9, pp. 1520–1533, 2004.

[39] B. T. Ingersoll, J. K. Ingersoll, P. DeFranco, and A. Ning, "UAV path-planning using Bezier curves and a receding horizon approach", *AIAA Modeling and Simulation Technologies Conference*. pp. 3675, 2016.

[40] H.K. Khalil, *Nonlinear Systems*. Prentice-Hall: Upper Saddle River, NJ, 2002.

Quan Quan received the B.S. and Ph.D. degrees in control science and engineering from Beihang University, Beijing, China, in 2004 and 2010, respectively. He has been an Associate Professor with Beihang University since 2013, where he is currently with the School of Automation Science and Electrical Engineering. His research interests include reliable flight control, swarm intelligence, vision-based navigation and health evaluation.

Rao Fu received the B.S. degree in control science and engineering from Beihang University, Beijing, China, in 2017. He is working toward to the Ph.D. degree at the School of Automation Science and Electrical Engineering, Beihang University (formerly Beijing University of Aeronautics and Astronautics), Beijing, China. His main research interests include UAV traffic control and swarm intelligence.

Kai-Yuan Cai Kai-Yuan Cai received the B.S., M.S., and Ph.D. degrees in control science and engineering from Beihang University (Beijing University of Aeronautics and Astronautics), Beijing, China, in 1984, 1987, and 1991, respectively. He has been a Full Professor with Beihang University since 1995. He is a Cheung Kong Scholar (Chair Professor), appointed by the Ministry of Education of China in 1999. His main research interests include software testing, software reliability, reliable flight control, ADA (autonomous, dependable, and affordable) control, and software cybernetics.